DESIGN ANALYSIS OF
A STEWART PLATFORM
FOR VEHICLE EMULATOR SYSTEMS

by

YOUHONG GONG

M.S., Materials Engineering

Shanghai Jiao Tong University

(1984)

Submitted to the Department of Mechanical Engineering

in partial fulfillment of the

requirements for the Degree of

MASTER OF SCIENCE

IN ENGINEERING

at the

Massachusetts Institute of Technology

January 1992

© 1992 Massachusetts Institute of Technology

Signature of Author_____

Department of Mechanical Engineering
January 18, 1992

Certified by _____

Harry West
Thesis Supervisor

Accepted by_____

Ain A. Sonin
Chairman, Departmental Graduate Committee

DESIGN ANALYSIS OF A STEWART PLATFORM FOR VEHICLE EMULATOR SYSTEMS

by

YOUHONG GONG

ABSTRACT

Design process of Stewart platform used as Vehicle Emulator System (VES) was investigated and various aspects which affect the basic behavior of the mechanism was examined. Two additional design considerations were proposed: stiffness and admittance emulation accuracy. The analysis reveals the relationship between the performance of VES and the components of the system, and it provides a deeper understanding of the behavior of the mechanism. Different kinematic models of the platform were discussed and compared. A new approach for numerically solving the forward kinematics was presented. Kinematic constraints of the platform are analyzed and a new algorithm was developed so that the leg interference problem could be solved more realistically.

A powerful graphical computer-aided procedure based on analysis was proposed and used as a valuable design tool to investigate the effects of geometry and constraints on the motion of the Stewart platform, to provide some important design information, such as platform's workspace, its joint angle and hydraulic flow rate etc., and to evaluate a proposed platform design. With the graphical simulation program, some design, control, error improvement and VES application guidelines could be obtained.

This research also attempted to establish an approach for correcting the position and orientation error of Stewart platform due to the variations of geometric parameters by either modifying desired leg length or modifying the desired position and orientation of the platform.

Thesis Supervisor: Dr. Harry West

Title: Assistant Professor of Mechanical Engineering

To My Wife Xiaoyan

ACKNOWLEDGEMENTS

TABLE OF CONTENTS

LIST OF FIGURES

LIST OF TABLES

CHAPTER 1

INTRODUCTION

1.1 OVERVIEW

Many applications of robotic manipulators today require or would benefit from the manipulator to operate on moving vehicle or other nonstationary environments. Such vehicles are compliant in comparison to stationary and rigid bases on which most conventional industrial manipulators mount. Examples of such applications include robots operating in space and mobile robotic system for nuclear environment. The base flexibility of mobile manipulator may seriously degrades system dynamic performance and a robot to operate from mobile base is subjected to arbitrary base motion disturbances. Such applications present challenging control problems not commonly found in conventional industrial manipulators. Research is undertaken at M.I.T. and a vehicle emulator was designed and built for experimental investigation of the behavior of manipulators operating in space, on compliant bases and in nonstationary environments. (see West et al [6], Dubowsky et al [7,9], Tanner [14] and Nguyen et al [27])

1.2 VEHICLE EMULATOR SYSTEM

The Vehicle Emulator System (VES) comprises a six-degree-of-
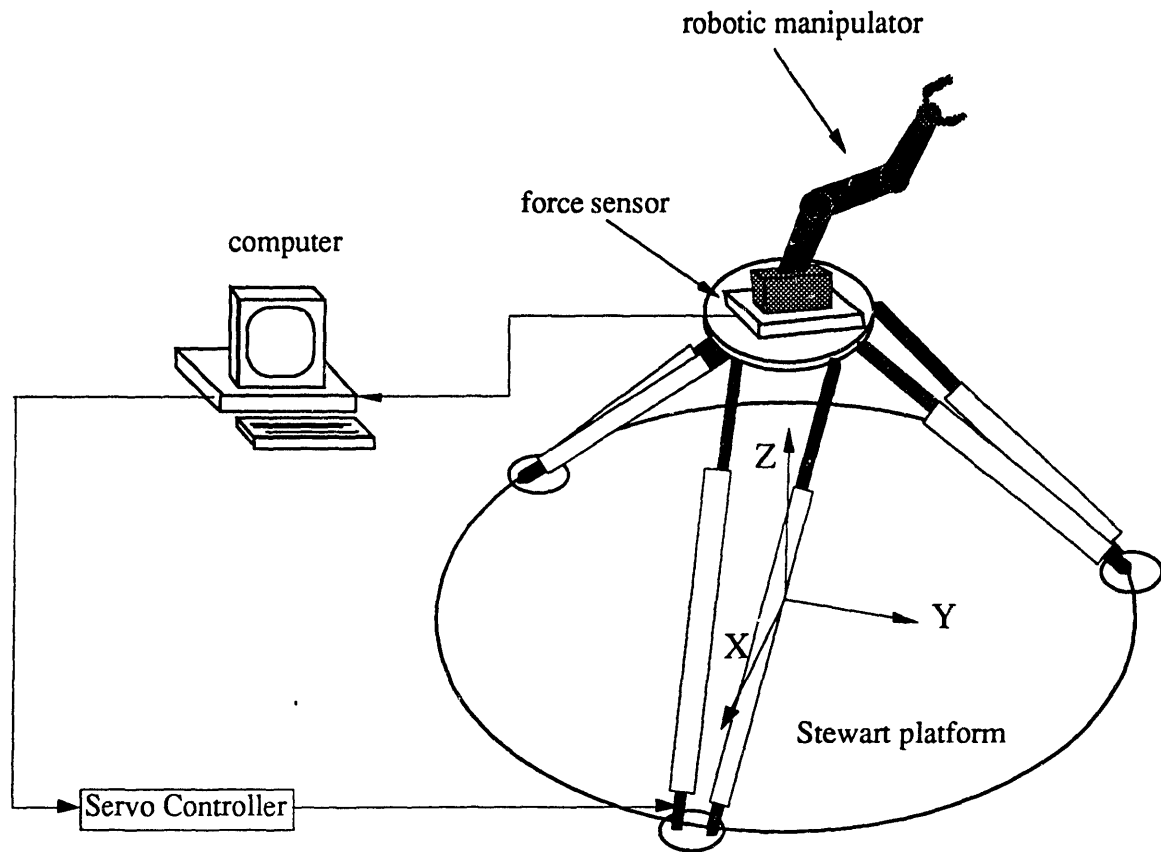
Figure 1.1 The Vehicle Emulator System

freedom, paralleled linked, hydraulic driven Stewart platform, a six-axis force/torque sensor and a control computer, as shown in Figure 1.1.

VES serve as a programmable test bed in experimental studies of robotic manipulator in space, on compliant bases and in nonstationary environments. With a robotic manipulator mounted on top of it, the platform acts as the dynamic system with which the manipulator interacts.

The force sensor measures the forces acting on the platform due to the motion of the manipulator. The platform controller model. the dynamic response of the system to those forces, i.e. the trajectory which the modeled system would follow if it were subjected to those forces, and controls the six hydraulic actuators to achieve the leg lengths corresponding to each desired platform motion and thus imposes the trajectory of the modeled system on platform. Because VES is programmable, the platform can emulate a wide range of different dynamic system.

1.3 CONTENTS AND ORGANIZATION

The design process of Stewart platform is studied. Two new design considerations for Stewart platform used as VES are discussed in Chapter 2. Detail accuracy and stiffness analyses of Stewart platform are also included. Chapter 3 presents the kinematic analysis of the platform. Different kinematic models are discussed, a new numerical method to solve the forward kinematics is given and a new approach to predict the interference between legs of the platform is presented. Chapter 4 described a computer graphical simulation program developed based on kinematic analysis, it is used as a design tool for the visualization of the mechanism, checking the design results and exploring different design alternatives. In Chapter 5, kinematics error correction problems including error calibration and tracking compensation are discussed. Chapter 6

concludes the investigation of design of Stewart platform use as VES and suggests areas where further work is needed. The appendices contain derivations which are too lengthy to be included in the main body.

CHAPTER 2

DESIGN SPECIFICATIONS

2.1 DESIGN CONSIDERATIONS

Stewart platform, which is constructed by connecting two plates to six adjustable legs, was originally designed as an aircraft simulator, and was also suggested for the application of machine tool, space vehicle emulator, etc. There have been many researchers who contributed greatly to the design and construction of this type of manipulators, especially, Fichter and McDowell [11,12] conceptually outlined the major criteria to design such manipulators. For Stewart platform used as VES, Fresco [3], Stelman [5], and Ismail [4] proposed a set of design specifications, including workspace requirements (vertical and horizontal range on motion, range of rotations about all axes), load capacity, bandwidth and maximum acceleration etc. Based on these design considerations, six geometric parameters corresponding to six degrees of freedom of the platform were determined and MIT first VES platform was designed and built. However, this set of design specifications was not complete. The performance of the platform designed only considering these specifications sometime was not so satisfactory, e.g. MIT first platform was floppy in horizontal direction.

In order to assure overall satisfactory performance, more aspects of the Stewart platform should be considered for its design. A simple one-degree-of-freedom model of VES was established and the characteristics of

simulation was analyzed, and an error factor was proposed to estimate the accuracy of the simulation and used as a design factor to measure the quality of the platform. Another important factor should be included in the set of design specifications is stiffness of the platform. Through detail investigation of static loading characteristics of the platform, the appropriate geometric parameters can be chosen so that the configuration of the platform can guarantee high rigidity in all directions.

2.2 ADMITTANCE EMULATION ACCURACY ANALYSIS

When Vehicle Emulator System is used to simulate a dynamic system, the tracking error of the platform is required to be smaller than certain number, in other words, the accuracy of the simulation should be specified. This accuracy is a measure of the quality of Stewart platform use as VES and should be taken into consideration when the platform is designed. However, using only a number value as accuracy without specifying other conditions is not correct for determining the quality of the simulation. We need to consider the relationship between the performance specifications of VES and simulation error, e.g., for simulating the motion of a robot working in space, the performance specifications will include the range and frequency of the robot motion, the masses of robot and satellite (the base system to be simulated) and the simulation time. Therefore, accuracy analysis is not only important but also necessary to find the fundamental characteristics of VES performance and thus to obtain insight

and some guidelines to the design process of Stewart platform.

Here we define the accuracy of VES as the tracking error of Stewart platform

$$\varepsilon = \frac{\text{tracking error}}{\text{the range of motion}}$$

Eqn. (2.1)

Relative error was used here, because absolute error is not a good measure for simulation, e.g, a 2 inch error for simulation with a range of 2 feet motion is large but maybe not so bad for a 20 feet motion.

There are many physical phenomena which cause a platform to deviate from its ideal tracking position. The stiffness of the platform affects the position accuracy of the system in the presence of static loads and disturbances. Detail stiffness analysis is given in next section. Kinematics error such as joint compliance, backlash and variation of geometric parameters of Stewart platform due to imperfect assembly and machining tolerances contribute to the inaccuracy of the tracking, however, these errors could be remedied either by good design and assembly or by kinematic error calibration and compensation. The mathematic model and error correction method for geometric parameters variation are discussed in Chapter 5.

The goal of VES is to make the platform simulate the response of a mechanical system of arbitrary dynamics which is subjected to the forces

acting on it. The performance in achieving this goal is affected by the accuracy of the trajectory generated by the admittance model and by the performance of the platform control system. The control of the hydraulic actuators is accomplished by analog servoamplifiers using proportional and derivative feedback. The model of the electrohydraulic actuator and controller design for VES were investigated by a lot of researchers. (West et al [6], Dubowsky et al [7,9], Fresco [3], Stelman [5], and Ismail [4]) Tracking error caused by PD controller, position sensor and servo actuator dynamics were found small enough to be ignored for simulation within the bandwidth of the system when controller gains were high. So, the major error is caused by inaccuracy of the trajectory generated by admittance model, particularly the accuracy of VES suffer from the error of the force data obtained by the computer from the force sensor.

For accuracy analysis here, it is assumed that the VES controller is good enough to drive the legs to reach exactly the desired lengths and this section focuses accuracy analysis on the errors caused from force sensor. Force sensor error can be divided into repeatable errors and stochastic errors. Repeatable errors include non-linearity and cross-talk which could be accounted for by force sensor characteristics tests and error calibration program. Stochastic errors include amplifier noise and drift, hysteresis, A/D quantization and temp-induced gain change. In order to simplify our accuracy analysis, force sensor errors were modelled in two types: offset error Δf_o which is constant, and gain error Δf_g which has a linear relation with the force the sensor measures.

$$\Delta f_o = \text{constant} = \beta f_{smax} \qquad \text{Eqn. (2.2a)}$$

$$\Delta f_g = \gamma f_s \qquad \text{Eqn. (2.2b)}$$

where β and γ are coefficients representing the quality of the force sensor, and f_s and f_{smax} are dynamic force the sensor measures and its maximum value respectively.

For simplicity and without loss of the generality, a one-degree-of-freedom model of VES, whose robot and platform move only along the vertical direction, is studied. The model is shown in Figure 2.1, where m_e is the mass of the robot and m is the mass of the base to be simulated. This base model only considering a pure mass is very useful for analysis
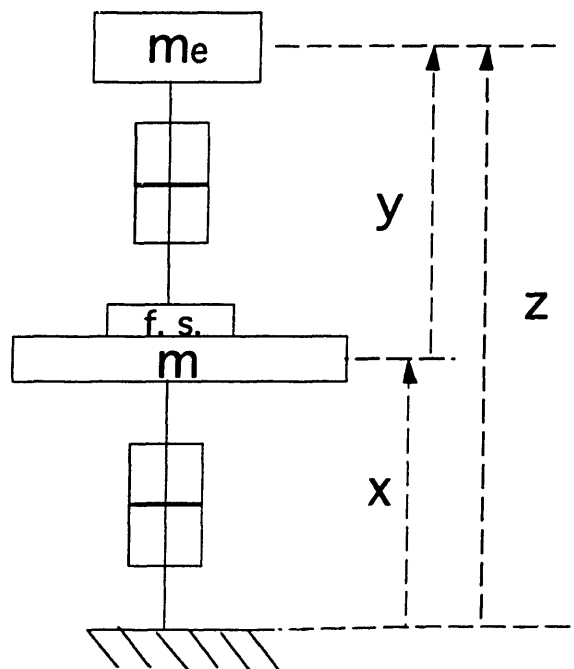
Figure 2.1 One-Degree-Of-Freedom Translation Model of VES

of robot working in space. A sinusoidal motion was chosen as typical robot motion type, i.e.,

$$y = Y\sin\omega t$$

Eqn. (2.3)

where Y and ω represents the amplitude and frequency of robot motion respectively. If we assume zero initial conditions and through the detail dynamic analysis (see Appendix 1.1), the relative error corresponding to two different force sensor error models are given as

$$\varepsilon_o = \frac{|\Delta z|}{|z_{max}|} = \beta \frac{m_e}{m} \omega^2 t^2$$

Eqn. (2.4a)

$$\varepsilon_g = \frac{\Delta z}{z} = -\gamma \frac{m_e}{m}$$

Eqn. (2.4b)

It is very obvious that the inaccuracy of VES simulation was caused by inaccuracy of the force data given to the admittance model from the force sensor, so quality of the force sensor is critical to VES performance. The results also shows that the ratio of robot mass to base mass determines the accuracy of the simulation, if the mass of the base is very large, the base system to be simulated is very similar to a rigid base case, so the error caused by the flexibility of the base will approach to zero. Eqn. (2.4a) shows that the offset error is proportional to square of the simulation time and frequency of robot motion, so for space simulation, the offset error will dominate and this error will limit the application of VES to simulate a space robot with fast motion or motion with a longer period .

$$J_e = m_e l^2$$

$$J = mr_g^2$$
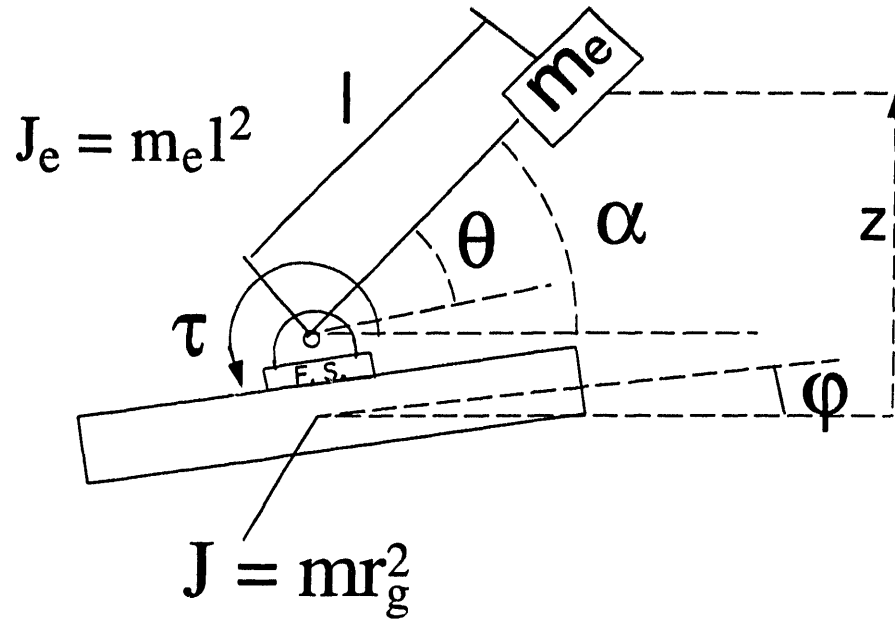
Figure 2.2 One-Degree-Of-Freedom Rotation Model of VES

If we modify this one-degree-of-freedom model to analyze VES rotational motion, as shown in Figure 2.2, and consider robot motion

$$\theta = \Theta \sin\omega t \qquad\qquad \text{Eqn. (2.5)}$$

Using the same initial conditions, and assuming small motion of the base, we obtain very similar results. (see Appendix 1.2)

$$\varepsilon_o = \frac{|\Delta\alpha|}{|\alpha_{max}|} = \beta\frac{J_e}{J}\omega^2 t^2 = \beta\frac{m_e l^2}{mr_g^2}\omega^2 t^2 \qquad\qquad \text{Eqn. (2.6a)}$$

$$\varepsilon_g = \frac{\Delta\alpha}{\alpha} = -\gamma\frac{J_e}{J} = -\gamma\frac{m_e l^2}{mr_g^2} \qquad\qquad \text{Eqn. (2.6b)}$$

The difference between these two models is that relative error for rotation motion is proportional to the ratio of moment of inertia instead of ratio of mass as in the case of translational motion.

Combining these two one-degree-of-freedom models, we can extend our model to a simple two-degrees-of freedom model, as shown in Figure 2.3, where the robot motion is still a pure sinusoidal rotation, but the base moves vertically and also rotates corresponding the force or torque the force sensor measures. If we assume small motion of base and zero initial conditions, and also for simplicity not considering the cross-talk effect between force sensor channels, the accuracy of VES could be obtained. (see Appendix 1.3)
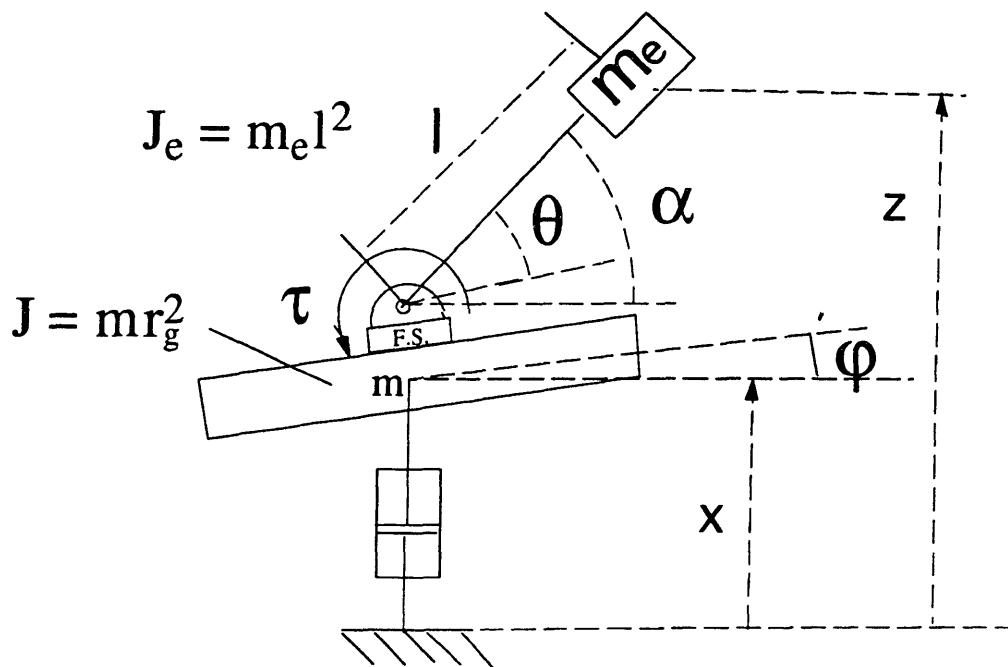
Figure 2.3 Simple Two-Degrees-Of-Freedom Model of VES

$$\varepsilon_0 = \frac{|\Delta z|}{|z_{max}|} = \beta \frac{m_e}{m} \omega^2 t^2 [1 + \frac{l^2}{r_g^2} + \frac{m_e l^2}{m r_g^2}]$$

Eqn. (2.7a)

$$\varepsilon_g = \frac{\Delta z}{z} = -\gamma \frac{m_e}{m} [1 + \frac{l^2}{r_g^2} + \frac{m_e l^2}{m r_g^2}]$$

Eqn. (2.7b)

The results shows that the both offset error or gain error consists of pure translational term, pure rotational term and a coupling term, which reflects the difficulty of accuracy analysis when the degrees of freedom of the system increases. However, this simple VES model relates the simulation error with masses or inertias of the system, quality of force sensor, frequency of robot motion and simulation time, and thus gives a rough measure of the accuracy of the simulation for a given system especially for the simulation of a robot working in space, and it provides very helpful information for selecting a proper force sensor.

For VES to simulate more general base system, e.g., the suspension system of a vehicle, the stiffness of the base system is a very important fact, so, it should be considered in the base model in addition to the inertial effect of the base, this two-degrees-of-freedom VES model is shown in Figure 2.4. In the model the stiffness of the base system includes both translational stiffness k and rotational stiffness k_r. Since stiffness exists in the base system, the base will produce a restoring force to balance the error force caused by the offset error of the force sensor. Therefore, in vehicle emulation case, the offset error is static and negligible and the gain error will dominate.
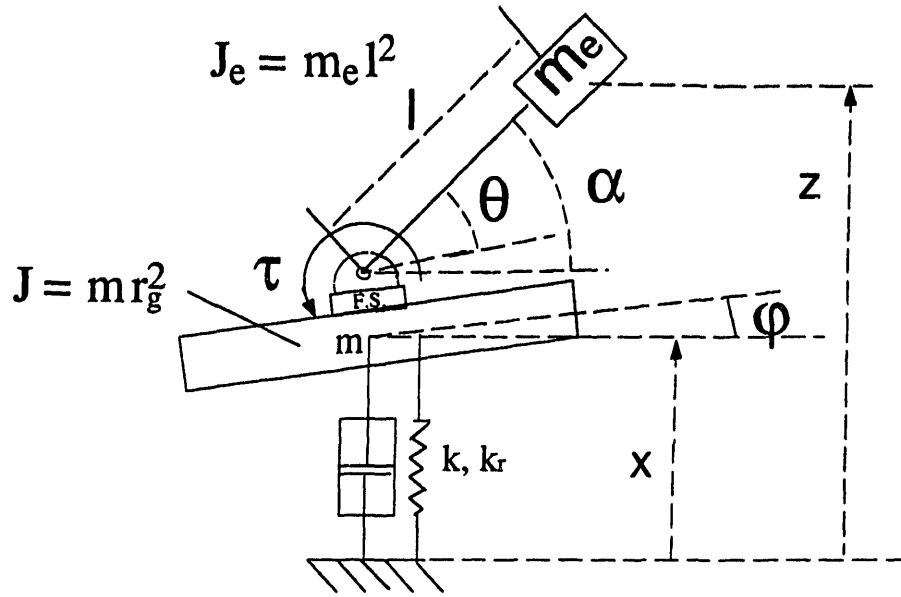
Figure 2.4 Two-Degrees-Of-Freedom Model of VES

Using the same method and same conditions, the accuracy of VES for the vehicle emulation could be obtained. (see Appendix 1.4)

$$\varepsilon_g = \frac{\Delta z}{z} = -\gamma\{\frac{Mm_e}{m+(1-M)m_e} + \frac{M_r m_e l^2}{mr_g^2+(1-M_r)m_e l^2} + \frac{(Mm_e)(M_r m_e l^2)}{[m+(1-M)m_e][mr_g^2+(1-M_r)m_e l^2]}\}$$

Eqn. (2.8)

where M and M_r are magnifying factors,

$$M = \frac{\omega^2}{\omega^2-\omega_n^2}$$

Eqn. (2.9a)

$$M_r = \frac{\omega^2}{\omega^2-\omega_{nr}^2}$$

Eqn. (2.9b)

and ω, ω_r are natural frequencies of the system

$$\omega_n^2 = \frac{k}{m+m_e}$$

<div align="right">Eqn. (2.10a)</div>

$$\omega_{nr}^2 = \frac{k_r}{J+J_e} = \frac{k_r}{mr_g^2+m_e l^2}$$

<div align="right">Eqn. (2.10b)</div>

This model is consistent with previous models, e.g., let $k\to0$, and $k_r\to0$, so, $\omega_n\to0$, $\omega_{nr}\to0$, $M\to1$ and $M_r\to1$, and the result will be the same as that of simple two-degrees-of-freedom model. If let $k\to0$ and $k_r\to\infty$, then $M\to1$ and $M_r\to0$, the result is exactly same as the result from simple one-degree-of-freedom translation model. Like previous models, the error of VES emulation due to the gain error of the force sensor consists of three terms: pure translation term, pure rotation term and a coupling term. The difference between space system and vehicle base system is that due to the stiffness of the base system, the error now is also related to the ratio of frequency of robot motion to the natural frequencies of the system. For a practical case, when $\omega \ll \omega_n$ and $\omega \ll \omega_{nr}$, we have

$$M \to -\frac{\omega^2}{\omega_n^2} \quad \text{and} \quad M_r \to -\frac{\omega^2}{\omega_{nr}^2}$$

<div align="right">Eqn. (2.11a)</div>

$$1-M \to 1+\frac{\omega^2}{\omega_n^2} \to 1 \quad \text{and} \quad 1-M_r \to 1+\frac{\omega^2}{\omega_{nr}^2} \to 1$$

<div align="right">Eqn. (2.11b)</div>

so the emulation error will approach to

$$\varepsilon_g = \frac{\Delta z}{z} = -\gamma m_e\omega^2[\frac{-1}{k} - \frac{l^2}{k_r} + \frac{m_e l^2\omega^2}{kk_r}]$$

<div align="right">Eqn. (2.12)</div>

Therefore, for very low frequency robot motion, the error will be dominated by quality of the force sensor, the mass or inertia of the robot, the stiffness of the base system and the frequency of the robot motion.

The accuracy analysis reveals the relationship between the simulation error, the components of Vehicle Emulation System and performance specifications of VES. It shows the dominant factors which affect the performance of VES in space simulation case or in vehicle simulation case, so it provides insight and some guidelines to the design process of Stewart platform. Although admittance emulation accuracy analysis results from simple models, same method can be generalized for a six-degrees-of-freedom case. And we should use the error factor as one of design considerations for Stewart platform because error analysis results could be used to approximately estimate the performance of VES, and Stewart platform thus designed will satisfy customer's performance requirements.

2.3 STIFFNESS ANALYSIS

Stiffness is a very important property of the manipulators. It determines the strength of the manipulators and positioning accuracy in the presence of disturbance and loads. Since it is very obvious that the stiffness of parallel manipulator like Stewart platform is much better than serial manipulator because the load of the platform are shared by its six legs, people will be prone to take it for granted that stiffness of Stewart platform is good enough and is not necessary to consider it as one of design

considerations. The shape of the platform thus determined without detail stiffness analysis resulted in a very floppy platform in horizontal direction and caused unexpected and dangerous collapse of the platform. Therefore, in order to design a platform with good stiffness in all directions within its workspace, a thorough analytical investigation of the stiffness of the Stewart platform should be made.

The idealized model for a symmetric Stewart platform is shown in Figure 2.5. The base and platform ball joints lie on the circles with radius R and r, respectively. Reference frame xyz is fixed to the platform and its position and orientation is described with respect to the inertial reference
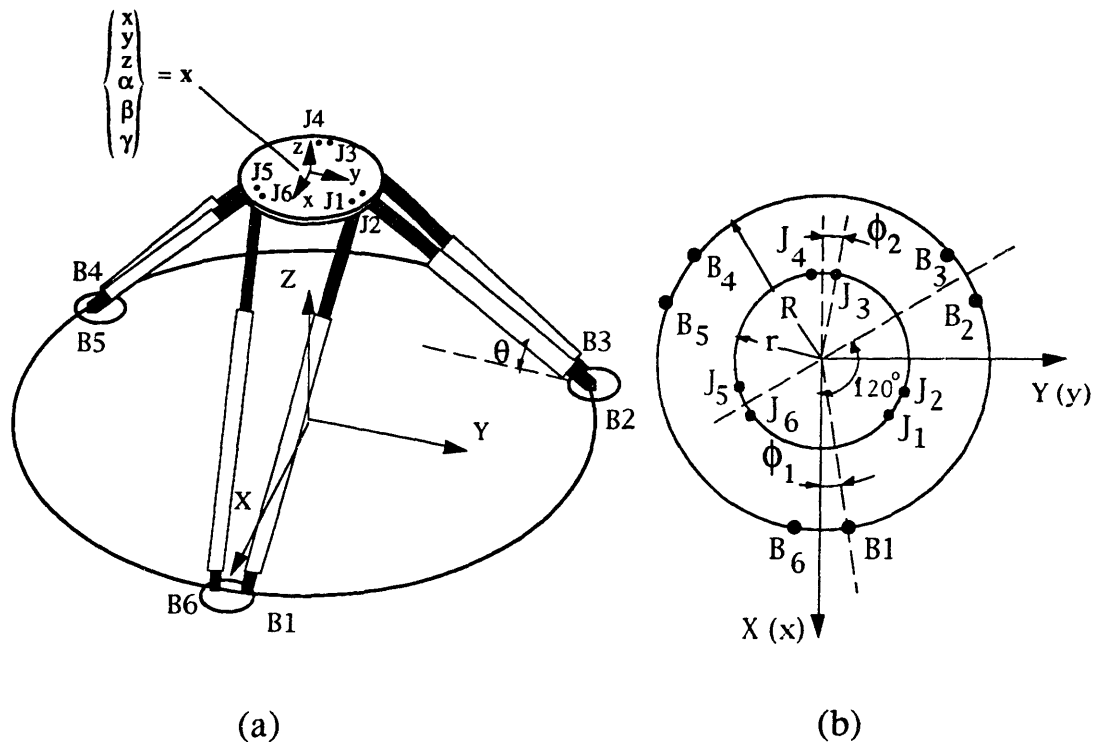

(a)   (b)

Figure 2.5 A Symmetric Stewart Platform

(a) Model of Platform   (b) Top View

frame XYZ, whose origin locates at the center of the base, by the end-effector position vector $\mathbf{x} = (x, y, z, \alpha, \beta, \gamma)^T$, where α, β, γ are roll, pitch and yaw rotations. Let $\mathbf{B_i} = \{X_{Bi}, Y_{Bi}, Z_{Bi}\}^T$, (i =1, 2, $\cdots$ 6), be the location of base joint center, defined as position vector with respect to XYZ frame and let $\mathbf{J_i} = \{x_{Ji}, y_{Ji}, z_{Ji}\}^T$ and $\mathbf{P_i} = (X_{Pi}, Y_{Pi}, Z_{Pi})^T$, (i = 1, 2, $\cdots$ 6) be the platform joint centers, defined as position vectors with respect to xyz and XYZ frames, respectively. In matrix form, the transformation from the xyz frame to XYZ frame is given by

$$\left\{ \frac{\mathbf{P_i}}{1} \right\} = [\mathbf{D}] \left\{ \frac{\mathbf{J_i}}{1} \right\}$$

Eqn. (2.13)

where [**D**] is a 4×4 displacement matrix, given by

$$[\mathbf{D}] = [\mathbf{D(x)}] = \left[\begin{array}{ccc|c} & & & x \\ \mathbf{R}_z(\gamma)\mathbf{R}_y(\beta)\mathbf{R}_x(\alpha) & & & y \\ & & & z \\ \hline 0 & 0 & 0 & 1 \end{array} \right] = \left[\begin{array}{ccc|c} & & & x \\ \mathbf{D_1} & \mathbf{D_2} & \mathbf{D_3} & y \\ & & & z \\ \hline 0 & 0 & 0 & 1 \end{array} \right]$$

Eqn. (2.14)

where

$$\mathbf{D_1} = \left\{ \begin{array}{c} D_{11} \\ D_{21} \\ D_{31} \end{array} \right\} = \left\{ \begin{array}{c} \cos\beta\cos\gamma \\ \cos\beta\sin\gamma \\ -\sin\beta \end{array} \right\}$$

Eqn. (2.15a)

$$\mathbf{D_2} = \left\{ \begin{array}{c} D_{12} \\ D_{22} \\ D_{32} \end{array} \right\} = \left\{ \begin{array}{c} \sin\alpha\sin\beta\cos\gamma - \cos\alpha\sin\gamma \\ \sin\alpha\sin\beta\sin\gamma + \cos\alpha\cos\gamma \\ \sin\alpha\cos\beta \end{array} \right\}$$

Eqn. (2.15b)

$$\mathbf{D_3} = \left\{ \begin{array}{c} D_{13} \\ D_{23} \\ D_{33} \end{array} \right\} = \left\{ \begin{array}{c} \cos\alpha\sin\beta\cos\gamma + \sin\alpha\sin\gamma \\ \cos\alpha\sin\beta\sin\gamma - \sin\alpha\cos\gamma \\ \cos\alpha\cos\beta \end{array} \right\}$$

Eqn. (2.15c)

If we define leg i as a vector $\mathbf{l_i}$, (i = 1, 2, $\cdots$, 6), we have

$$\mathbf{l_i} = \begin{Bmatrix} l_{iX} \\ l_{iY} \\ l_{iZ} \end{Bmatrix} = \mathbf{P_i} - \mathbf{B_i}$$

<div align="right">Eqn. (2.16a)</div>

or described in xyz frame,

$$\mathbf{l_i} = \begin{Bmatrix} l_{ix} \\ l_{iy} \\ l_{iz} \end{Bmatrix} = \begin{Bmatrix} \mathbf{l_i \cdot D_1} \\ \mathbf{l_i \cdot D_2} \\ \mathbf{l_i \cdot D_3} \end{Bmatrix}$$

<div align="right">Eqn. (2.16b)</div>

substitute Eqn. (2.13) - Eqn. (2.15) into Eqn. (2.16a), we obtain

$$\mathbf{l_i} = \begin{Bmatrix} l_{iX} \\ l_{iY} \\ l_{iZ} \end{Bmatrix} = \begin{Bmatrix} D_{11}x_{Ji} + D_{12}y_{Ji} + D_{13}z_{Ji} + x - X_{Bi} \\ D_{21}x_{Ji} + D_{22}y_{Ji} + D_{23}z_{Ji} + y - Y_{Bi} \\ D_{31}x_{Ji} + D_{32}y_{Ji} + D_{33}z_{Ji} + z \end{Bmatrix}$$

<div align="right">Eqn. (2.17)</div>

and the length of leg i, (i = 1, 2, $\cdots$, 6), is given by

$$l_i = |\mathbf{P_i} - \mathbf{B_i}| = \sqrt{l_{iX}^2 + l_{iY}^2 + l_{iZ}^2}$$

<div align="right">Eqn. (2.18)</div>

and leg vector is defined as $\mathbf{l}$, given by

$$\mathbf{l} = \begin{Bmatrix} l_1 \\ l_2 \\ l_3 \\ l_4 \\ l_5 \\ l_6 \end{Bmatrix} = \mathbf{l(x)}$$

<div align="right">Eqn. (2.19)</div>

According to the principles of virtual work, using the method very similar to serial manipulator, it can be proved that there is a relationship between the leg force and end-effector force. (Asada and Slotine [1])

$$\{F\}_x = [J]^T \{F\}_l \qquad\qquad\text{Eqn. (2.20)}$$

where

$$\{F\}_x = \begin{Bmatrix} f_x \\ f_y \\ f_z \\ m_x \\ m_y \\ m_z \end{Bmatrix} \qquad\qquad \{F\}_l = \begin{Bmatrix} f_1 \\ f_2 \\ f_3 \\ f_4 \\ f_5 \\ f_6 \end{Bmatrix} \qquad\qquad\text{Eqn. (2.21)}$$

are end-effector force vector and leg force vector respectively, as shown in Figure 2.6. $[J]^T$ is the transpose of the manipulator Jacobian matrix, which is defined as

$$[J] = \left[\frac{\partial l}{\partial x}\right] = \begin{bmatrix} \dfrac{\partial l_1}{\partial x} & \dfrac{\partial l_1}{\partial y} & \cdots & \dfrac{\partial l_1}{\partial \gamma} \\[2mm] \dfrac{\partial l_2}{\partial x} & \dfrac{\partial l_2}{\partial y} & \cdots & \dfrac{\partial l_2}{\partial \gamma} \\[2mm] & & \cdots & \\[1mm] \dfrac{\partial l_6}{\partial x} & \dfrac{\partial l_6}{\partial y} & \cdots & \dfrac{\partial l_6}{\partial \gamma} \end{bmatrix} \qquad\qquad\text{Eqn. (2.22)}$$

If we neglect gravity and friction, we can relate the, leg force to leg deflection $\Delta l = [\Delta l_1, \Delta l_2, \cdots, \Delta l_6]^T$ by the individual stiffness, which is modeled as

$$f_i = k_i \, \Delta l_i \qquad\qquad\text{Eqn. (2.23)}$$

where f_i is the force produced by leg i and Δl_i is the deflection of leg i. k_i is the spring constant. Eqn (2.6) could be rewritten in vector form

End-effector
Position

$$\begin{Bmatrix} x \\ y \\ z \\ \alpha \\ \beta \\ \gamma \end{Bmatrix} = \mathbf{x}$$

$$\begin{Bmatrix} f_x \\ f_y \\ f_z \\ m_x \\ m_y \\ m_z \end{Bmatrix} = \{\mathbf{F}\}_x$$

End-effector
Force

$$\begin{Bmatrix} f_1 \\ f_2 \\ f_3 \\ f_4 \\ f_5 \\ f_6 \end{Bmatrix} = \{\mathbf{F}\}_l \quad \text{Leg Force}$$
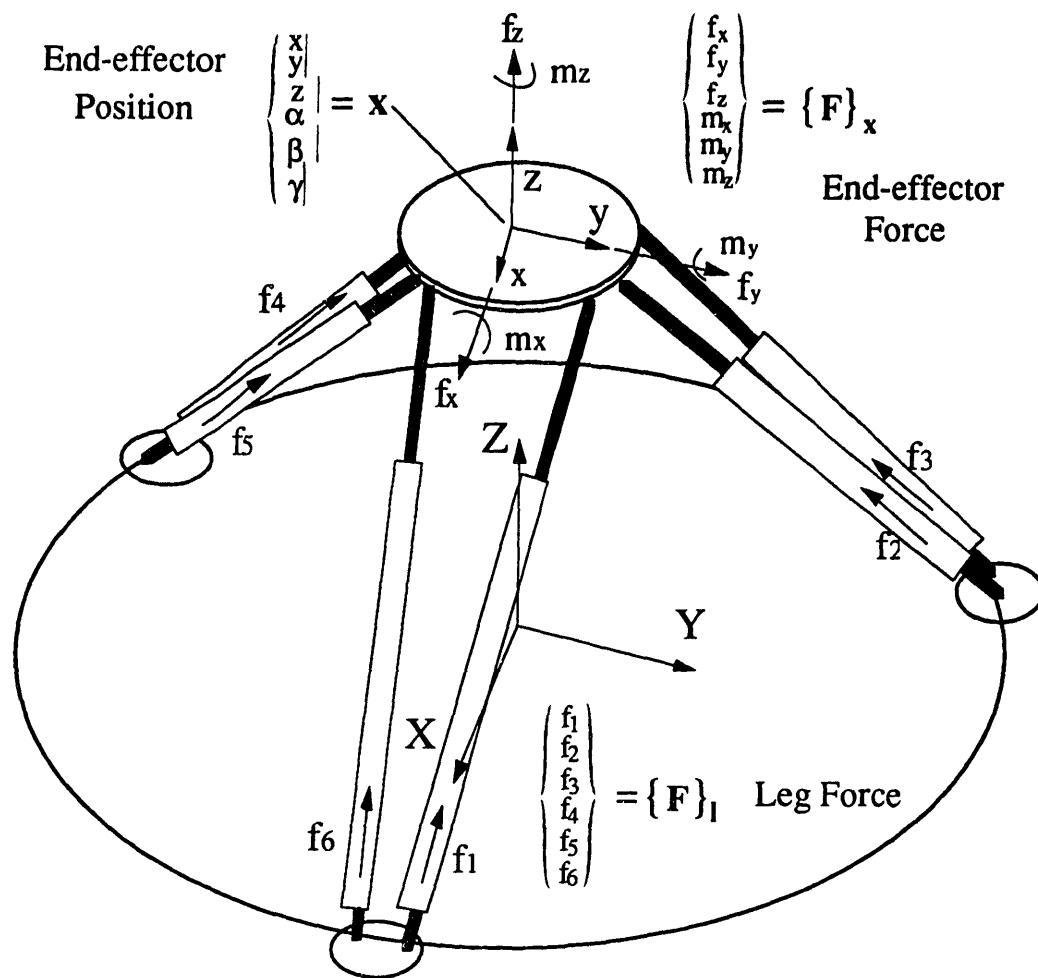
Figure 2.6 Forces Applied on Platform

$$\{\mathbf{F}\}_l = [\mathbf{K}]\,\Delta l \qquad\qquad \text{Eqn. (2.24)}$$

where [K] is 6×6 diagonal matrix given by

$$[K] = \begin{bmatrix} k_1 & & & \\ & k_2 & & 0 \\ & & \ddots & \\ 0 & & & k_6 \end{bmatrix} \qquad \text{Eqn. (2.25)}$$

Since Jacobian matrix [J] relates platform deflection Δx and leg deflection Δl by

$$\Delta l = [J]\,\Delta x \qquad \text{Eqn. (2.26)}$$

so from Eqn. (2.16) we obtain

$$\{F\}_l = [K][J]\,\Delta x \qquad \text{Eqn. (2.27)}$$

substitute Eqn. (2.19) into Eqn. (2.13), we obtain

$$\{F\}_x = [S]\,\Delta x \qquad \text{Eqn. (2.28)}$$

where

$$[S] = [J]^T[K][J] \qquad \text{Eqn. (2.29)}$$

Thus the deflection of the platform is related the external force applied to the platform by the 6×6 matrix [S]. The matrix [S] is called the stiffness matrix of the platform.

Since [S] consists of individual leg stiffness and Jacobian matrix, it is configuration dependent. Based on above analysis, stiffness at any point throughout the workspace of the platform can be obtained.

For a symmetric Stewart platform as shown in Figure 2.5, the locations of the joints are given by

$$X_{B1} = R\cos\phi_1; \qquad Y_{B1} = R\sin\phi_1;$$

$$X_{B2} = -R\sin(\frac{\pi}{6} - \phi_1); \qquad Y_{B2} = R\cos(\frac{\pi}{6} - \phi_1);$$

$$X_{B3} = -R\sin(\frac{\pi}{6} + \phi_1); \qquad Y_{B3} = R\cos(\frac{\pi}{6} + \phi_1);$$

$$X_{B4} = X_{B3}; \qquad Y_{B4} = -Y_{B3};$$

$$X_{B5} = X_{B2}; \qquad Y_{B5} = -Y_{B2};$$

$$X_{B6} = X_{B1}; \qquad Y_{B6} = -Y_{B1};$$

$$x_{J1} = r\sin(\frac{\pi}{6} + \phi_2); \qquad y_{J1} = r\cos(\frac{\pi}{6} + \phi_2);$$

$$x_{J2} = r\sin(\frac{\pi}{6} - \phi_2); \qquad y_{J2} = r\cos(\frac{\pi}{6} - \phi_2);$$

$$x_{J3} = -r\cos\phi_2; \qquad y_{J3} = r\sin\phi_2;$$

$$x_{J4} = x_{J3}; \qquad y_{J4} = -y_{J3};$$

$$x_{J5} = x_{J2}; \qquad y_{J5} = -y_{J2};$$

$$x_{J6} = x_{J1}; \qquad y_{J6} = -y_{J1};$$

$$Z_{Bi} = z_{Ji} = 0 \qquad (\ i = 1, 2, \cdots, 6) \qquad \text{Eqn. (2.30)}$$

We define x_i^* and y_i^*, ($i = 1, 2, \cdots, 6$), by

$$x_i^* = x_{Ji} - X_{Bi} \qquad \text{Eqn. (2.31a)}$$

$$y_i^* = y_{Ji} - Y_{Bi} \qquad \text{Eqn. (2.31b)}$$

and the following relations can be proved (see Appendix 2.1),

$$\sum_{i=1}^{6} X_{Bi} = \sum_{i=1}^{6} Y_{Bi} = \sum_{i=1}^{6} x_{Ji} = \sum_{i=1}^{6} y_{Ji} = 0 \qquad \text{Eqn. (2.32a)}$$

$$\sum_{i=1}^{6} x_i^* = \sum_{i=1}^{6} y_i^* = \sum_{i=1}^{6} x_i^* y_i^* = 0 \qquad \text{Eqn. (2.32b)}$$

$$\sum_{i=1}^{6} (x_i^*)^2 = \sum_{i=1}^{6} (y_i^*)^2 = 3[r^2 + R^2 - 2rR\sin(\pi/6 + \varphi 1 + \varphi 2)] = 3r^{*2} \qquad \text{Eqn. (2.32c)}$$

$$\sum_{i=1}^{6} (x_{Ji})^2 = \sum_{i=1}^{6} (y_{Ji})^2 = 3r^2 \qquad \text{Eqn. (2.32d)}$$

$$\sum_{i=1}^{6} (X_{Ji})^2 = \sum_{i=1}^{6} (Y_{Ji})^2 = 3R^2 \qquad \text{Eqn. (2.32e)}$$

$$\sum_{i=1}^{6} x_{Ji} X_{Bi} = \sum_{i=1}^{6} y_{Ji} Y_{Bi} = -\frac{3}{2}(r^{*2} - r^2 - R^2) \qquad \text{Eqn. (2.32f)}$$

$$\sum_{i=1}^{6} x_{Ji} Y_{Bi}^2 = \sum_{i=1}^{6} y_{Ji} X_{Bi} Y_{Bi} = -\frac{3}{2}rR^2\sin(\pi/6 + \varphi 2 - 2\varphi 1) \qquad \text{Eqn. (2.32g)}$$

$$\sum_{i=1}^{6} y_{Ji}^2 X_{Bi} = \sum_{i=1}^{6} x_{Ji} y_{Ji} Y_{Bi} = \frac{3}{2}r^2 R\sin(\pi/6 + \varphi 1 - 2\varphi 2) \qquad \text{Eqn. (2.32h)}$$

$$\sum_{i=1}^{6} y_{Ji}^2 X_{Bi}^2 = \sum_{i=1}^{6} x_{Ji}^2 Y_{Bi}^2 = \frac{3}{8}r^2 R^2[3 + 2\cos^2(\varphi 1 + \varphi 2) - \sqrt{3}\sin(2\varphi 1 + 2\varphi 2)] \qquad \text{Eqn. (2.32i)}$$

$$\sum_{i=1}^{6} x_{Ji}y_{Ji}X_{Bi}Y_{Bi} = -\frac{3}{4}r^2R^2\sin(\pi/6 - 2\varphi1 - 2\varphi2)$$

Eqn. (2.32j)

From Eqn. (2.17), (2.18) and (2.30), each term of Jacobian matrix [J] can be given by (see Appendix 2.2),

$$\frac{\partial l_i}{\partial x} = \frac{l_{ix}}{l_i} = \frac{D_{11}x_{Ji} + D_{12}y_{Ji} + x - X_{Bi}}{l_i}$$

Eqn. (2.33a)

$$\frac{\partial l_i}{\partial y} = \frac{l_{iY}}{l_i} = \frac{D_{21}x_{Ji} + D_{22}y_{Ji} + y - Y_{Bi}}{l_i}$$

Eqn. (2.33b)

$$\frac{\partial l_i}{\partial z} = \frac{l_{iZ}}{l_i} = \frac{D_{31}x_{Ji} + D_{32}y_{Ji} + z}{l_i}$$

Eqn. (2.33c)

$$\frac{\partial l_i}{\partial \alpha} = \frac{y_{Ji}(l_i \cdot D_3)}{l_i} = y_{Ji}\frac{l_{iz}}{l_i}$$

Eqn. (2.33d)

$$\frac{\partial l_i}{\partial \beta} = \frac{l_i \cdot (y_{Ji}\sin\alpha D_1 - x_{Ji}\sin\alpha D_2 - x_{Ji}\cos\alpha D_3)}{l_i}$$

Eqn. (2.33e)

$$\frac{\partial l_i}{\partial \gamma} = \frac{l_i \cdot [x_{Ji}\cos\beta(\cos\alpha D_2 - \sin\alpha D_3) - y_{Ji}(\cos\alpha\cos\beta D_1 + \sin\beta D_3)]}{l_i}$$

Eqn. (2.33f)

Based on above analysis, for platform at home position, where x = $\{0, 0, z_0, 0, 0, 0\}$, and due to symmetry of the configuration, the leg length $l_i = l_0$, (i = 1, 2, $\cdots$, 6), and we assume that the individual stiffness of each leg is same, i.e., $k_i = k$, (i = 1, 2, $\cdots$, 6), using Eqn. (2.28,2.29,2.32,2.33), we can calculate [J] and [S], and some useful results are obtained, as shown in Figure 2.7. (see Appendix 2.3 for detail)

(i) At home position, the stiffness in horizontal direction is the same, i.e., it is independent of direction. And both the vertical or horizontal stiffness of the platform depends only on its height z_0, or θ, one of the design parameters. Here $z_0 = l_0\sin\theta$, as shown in Figure 2.5. The vertical stiffness increases with the increase of θ, but, horizontal stiffness decreases when θ is larger.

(ii) At home position, the maximum stiffness in horizontal direction is just half of that in vertical direction.

(iii) $\theta = 45°$ is the half point for stiffness both in horizontal or vertical direction. Therefore, the design parameter θ should be chosen not far away from $45°$.
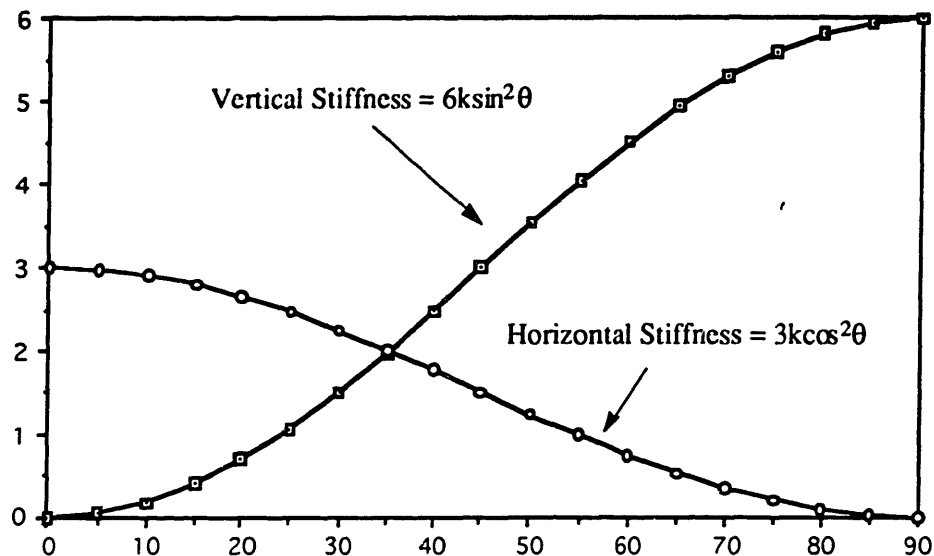
Figure 2.7 Stiffness of the Platform at Home Position

This stiffness analysis explains why the old platform is so floppy in horizontal direction, because the design parameter θ was 74°, so the ratio of vertical stiffness to horizontal stiffness for the previous platform was about 20. The stiffness analysis also provides us some guidelines for determining the shape of the platform in terms of the locations of the joint attachments to base, in other words, for a given home height of the platform, z_0, another design parameter ϕ_1 should be chosen as small as possible, so that angle θ could be smaller to improve the horizontal stiffness.

Since the stiffness of the platform is Jacobian matrix dependent, it will be zero at least in one direction if Jacobian matrix [J] degenerates at singular positions of the platform. So the end-effector will deflect in that direction with no force or moment induced to resist this motion. Platform will gain an extra degree of freedom and may crash.

CHAPTER 3

KINEMATIC ANALYSIS

3.1 KINEMATIC MODELS

The purpose of investigation of kinematics of Stewart platform is to establish analytical methods and develop computer-aided procedure capable of analyzing the basic kinematic characteristics of this mechanism, such as its extreme range of motion and workspace, and recognizing its physical limitations, so that we can obtain some design and application guidelines for this type of manipulator.

The first step of kinematic analysis is to develop a kinematic model of the platform. Several kinematic models of the platform were proposed and a lot of researchers, such as Do [2], Fresko [3], Powell [10], Fichter and McDowell [12], McCallion and Truong [13], and Yang and Lee [17], did great contributions to the developments and applications of these models. Three models, among others, are mostly accepted and used.

Model 1: This model is described in Chapter 2, see Figure 2.2. Using Cartesian coordinates and homogeneous transform matrix, the displacement of the top plate (its position and orientation) is described with respect to inertia frame XYZ. The locations of top joints described as points in Cartesian space xyz are mapped to inertia Cartesian space XYZ and each leg can be represented by a Cartesian vector in XYZ space.

Z

Ii

$J_I (P_I)$

Mi

Y

X

$$\text{Leg i} \quad U_I = \begin{Bmatrix} l_{ix} \\ l_{iy} \\ l_{iz} \\ M_{ix} \\ M_{iy} \\ M_{iz} \end{Bmatrix}$$

Bi

ISA
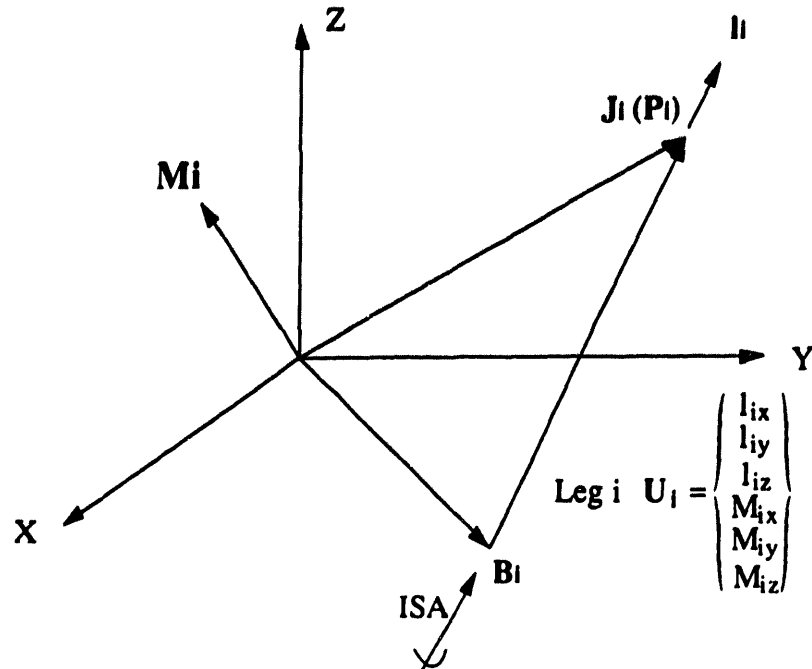
Figure 3.1 Plücker Coordinates of Leg i

Model 2: The displacement of top platform and the locations of joint attachment are described in the same way as model 1. But, the legs are represented by Plücker coordinates, as depicted in Figure 3.1. The legs may be determined from any two distinct points on the line. The vector l_i, (i = 1, 2, ···, 6), lies along the line in the direction of leg i. Vector M_i is perpendicular to the plane containing the line i and the origin, so it is the moment of vector l_i about the origin. The vector l_i and M_i are assembled into the plücker coordinates vector U_i, given by

$$U_i = \begin{Bmatrix} l_{ix} \\ l_{iy} \\ l_{iz} \\ M_{ix} \\ M_{iy} \\ M_{iz} \end{Bmatrix}$$

Eqn. (3.1)

According to skew theory, at every instant during the motion of a body in space, there is an instantaneous screw axis (ISA) and the translational velocity v and angular velocity ω has a relation

$$v = h \, \omega \qquad\qquad \text{Eqn. (3.2)}$$

where h is the pitch. From skew theory, given the displacement and velocity of the platform, the velocities of the legs can be obtained. (see Fichter [11])

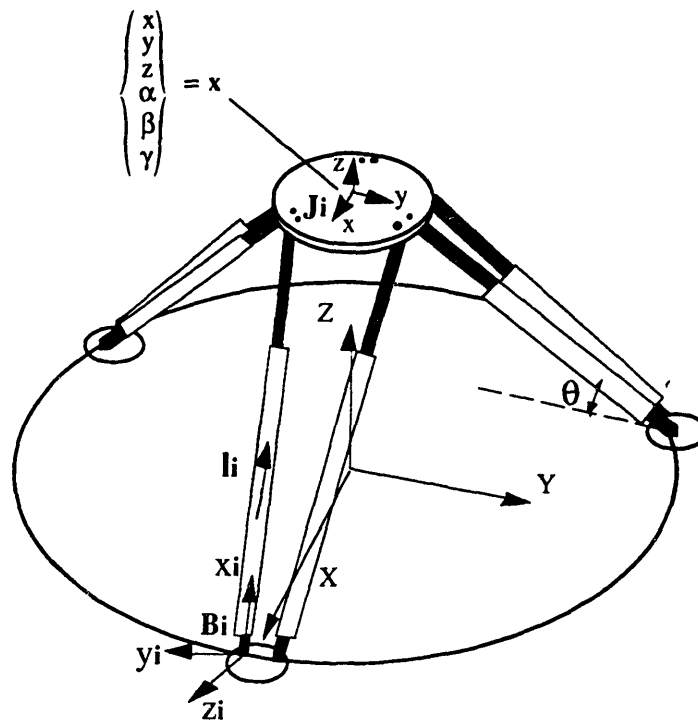Model 3: This model is based on model 1. In addition to reference

Figure 3.2 Local Coordinates of Leg i

frames XYZ and xyz, Cartesian reference frame xyz_i, (i = 1, 2, $\cdots$, 6), is denoted as the local coordinates system fixed to leg i, as shown in Figure 3.2.

The origin of xyz_i is joint B_i and the axis x_i points towards joint J_i. The y_i axis is parallel to the cross product of -Z and l_i, and the axis z_i is defined by the right hand rule. Thus the motion of the leg i could be described by the reference frame xyz_i with respect to XYZ.

These three models are essentially the same, because they represent the same physical plant, just different in the mapping of the coordinates from one vector space to another one. However, a different model is more than just a varying representation of the platform, it can elucidate aspects of the underlying theory and suggest results that might be otherwise go unsolvable or unnoticed. Model 1 is an easy, straight-forward and efficient model for calculation of inverse or forward kinematics and for real time control of the platform. But, model 1 does not consider the rotation of the legs, so generally it could not be extended to a dynamic model. Model 2 takes consideration of the rotation of the legs and skew theory provides qualitative and physical insight into underlying geometry of the platform while quantitative calculation could be easier via coordinate map. Model 2 is used to calculate the rate change of the leg velocity, to determine the singular positions of the platform and to do dynamic analysis based on screw theory. However, the calculation using model 2 is complicated and time consuming. Model 3 puts emphasis on each leg, so it is easy to

analyze relative motion of the legs, such as the interference problem between the legs, and a local coordinates system is more convenient to use for each part of the platform as a free body, so that the equation of motion of the system can be formulated for dynamic analysis.

3.2 FORWARD KINEMATICS

There are two types of kinematic analysis, known as inverse and forward kinematics, very important and useful in the design and control of Stewart platform. The inverse kinematics calculates the leg lengths l_i (i = 1, 2, ···, 6), corresponding to a given end-effector position x. Its solution is straight-forward and unique, and is discussed in Chapter 2, Eqn. (2.17). (also see McCallion and Truong [13], Fichter [11], Fresco [3]) The forward kinematics transforms leg coordinates into the reference coordinates of the end-effector, i.e. given the lengths of six variable legs, l, find the transformation of coordinates representing the position and orientation of the top plate, x, with respect to inertia reference frame XYZ. By contrast to inverse kinematics, forward kinematics is neither well behaved nor easily described.

Although the inverse kinematics of Stewart platform has been extensively studied, no closed form solutions to the forward kinematics have been presented in literature. Landsberger [36] studied the existence and solvability of the forward kinematics problems. Zhang and Song [21] explored the condition under which the closed form solutions of forward

kinematics of parallel platform. Griffs and Duffy [18] investigated a special form of Stewart platform and reduced the forward kinematics solution to a sixteenth degree polynomial after eliminations of unknowns. Nunua and Waldron [19] studied the same problem by a different approach and obtained the similar result.

It is very difficult to solve the forward kinematics by directly invert Eqn. (2.18), because it involves simultaneous solution of six nonlinear quadratic equations together with constraints equations. However, the forward kinematics is required for dynamic simulation, workspace analysis, error correction and other applications. So, that lead the researchers to seek an iterate numerical method to solve the forward kinematics. (Ismail [4], Cleary and Arai [22], Nguyen et al [27])

Two numerical techniques were often used. The first is a direct integration. Given $\mathbf{dl} = [\mathbf{J}] \, \mathbf{dx}$, then

$$\mathbf{x} = \int_{\mathbf{l_0}}^{\mathbf{l}} [\mathbf{J}]^{-1} \mathbf{dl} + \mathbf{x_0}$$

Eqn. (3.3)

where $\mathbf{x_0}$ is initial guess of $\mathbf{x}$, $\mathbf{l_0}$ is corresponding leg length vector. The second method is using multidimensional Newton-Raphson procedure. From Chapter 2, we know that the inverse kinematics can give the desired leg length $\mathbf{l_d}$ corresponding to a given position of the platform $\mathbf{x_d}$, so, we define a multidimensional function

$$f(x) = \begin{pmatrix} f_1(x) \\ f_2(x) \\ \vdots \\ f_6(x) \end{pmatrix} = \begin{pmatrix} l_1 - l_{d1} \\ l_2 - l_{d2} \\ \vdots \\ l_6 - l_{d6} \end{pmatrix} = l - l_d$$

Eqn. (3.4)

In the neighborhood of x, each of the functions f_i, ($i = 1, 2, \cdots, 6$), can be expanded in Taylor series. By neglecting higher order terms and letting f(x) equal to zero,

$$f(x + \Delta x) \cong f(x) + \frac{\partial f}{\partial x} \Delta x = f(x) + \frac{\partial l}{\partial x} \Delta x$$
$$= f(x) + [J] \Delta x$$

Eqn. (3.5)

therefore, we have an iterate formula for the forward kinematics,

$$\Delta x = -[J]^{-1} f(x) = -[J]^{-1} \{ l - l_d \}$$

Eqn. (3.6)

Although these two methods can obtain rather accurate results depending on a good initial guess of the position x_0, both methods need the successive calculation of a 6×6 inverse Jacobian matrix $[J]^{-1}$ and lower efficiency degrades the methods, especially for real-time applications. Also, these methods could fail when Jacobian matrix is singular.

There are some other numerical methods which could be used to solve the forward kinematics, such as using a fixed $[J]^{-1}$, using difference quotients instead of partial derivatives in calculation of Jacobian matrix or using some multidimensional optimization algorithms. But, these methods

could not improve the efficiency of the calculation without losing the accuracy of the results.

The following method for forward kinematics was developed and is shown in Figure 3.3. For the given leg lengths, which are physically realizable, we suppose that the platform consisting of pairs of springs and dampers is at equilibrium state. Any state deviated from this equilibrium
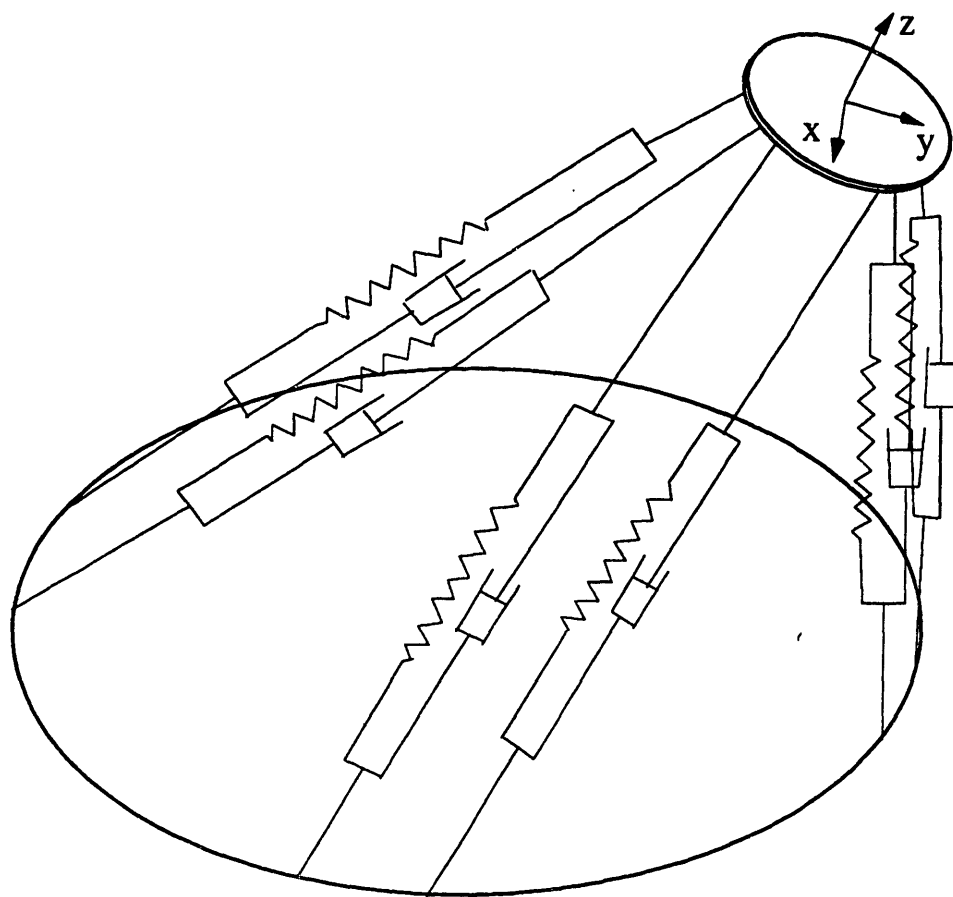

Figure 3.3 Model of Platform for Forward Kinematics

state will cause the deflections of the virtual springs, which are the differences between the current leg lengths and given leg lengths. The platform driven by the corresponding spring forces will move towards the equilibrium position until the disappearance of deflections of the springs. Lyapunov stability theory is used here to derive the numerical forward kinematics algorithm. For simplicity, we only discuss the model where the effect of dampers are neglected. For a desired leg length l_d, let x be the current desired end-effector position estimate corresponding to the state off the equilibrium position, and define the current error, i.e. the virtual spring deflections as

$$\tilde{l} = \Delta l = l(x) - l_d$$

<div align="right">Eqn. (3.7)</div>

Let us then select a Lyapunov function candidate as

$$V = \frac{1}{2}\tilde{l}^T[K_p]\tilde{l}$$

<div align="right">Eqn. (3.8)</div>

where $[K_p]$ is a positive definite matrix. Differentiating Eqn. (3.8) and substitute Eqn. (2.26), we get

$$\dot{V} = \tilde{l}^T[K_p]\dot{\tilde{l}} = \tilde{l}^T[K_p]\dot{l} = \tilde{l}^T[K_p][J]\Delta x$$

<div align="right">Eqn. (3.9)</div>

so if we chose

$$\Delta x = -[J]^{-1}\tilde{l}$$

<div align="right">Eqn. (3.10)</div>

---

then

$$\dot{V} = -\tilde{i}^T[K_p]\tilde{i} \le 0$$

Eqn. (3.11)

This is essentially the multidimensional Newton-Raphson method. However, if we chose

$$\Delta x = -[J]^T[K_p]^T\tilde{i}$$

Eqn. (3.11)

then, we obtain

$$\dot{V} = -\tilde{i}^T[K_p][J][J]^T[K_p]^T\tilde{i}$$
$$= -\Delta x^T \cdot \Delta x \quad \le 0$$

Eqn. (3.12)

For this method, it is not required to calculate the time consuming inverse Jacobian matrix , $[J]^{-1}$, and it locally guarantees the convergence of the algorithm, because we use the virtual mechanical energy V and platform as a virtual passive physical system will eventually goes to its equilibrium state. However, the number of iterations, i.e. the time of calculation is dependent of the initial end-effector position guess x_0. If Jacobian matrix is singular, this method will lead Δx "stuck" at a non-zero value, but a skew symmetric matrix will be helpful to remedy the situation.

3.3 KINEMATIC CONSTRAINTS

In order to investigate the effect of configuration on workspace, analysis of kinematic constraints is necessary in the design process of Stewart platform and it is also imperative for a safe operation of the VES

system. The Stewart platform controller should ensure any position of the end-effector in a trajectory from breaking the kinematic constraints or being beyond the workspace. Stelman [5] investigated three types of kinematic constraints of Stewart platform: maximum and minimum actuator lengths, limits of rotation of joints and interference of the legs. A new approach here was developed for the interference problem.

Interference of legs occurs in a variety of platform positions. Obvious example is when platform rotates about its z axis at certain angle, pairs of adjacent legs will hit each other. This will not only limit the workspace of the platform, but also dangerously cause the damage of the platform. Stelman [5] used a cylinder model, as shown in Figure 3.4, to
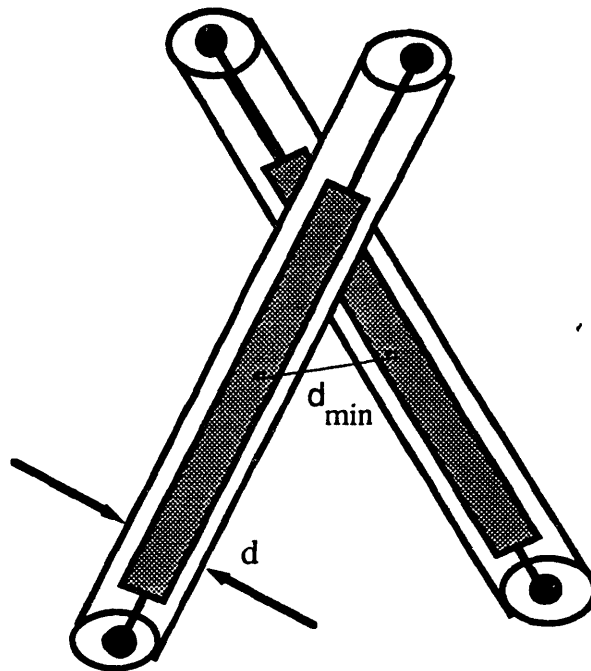
Figure 3.4 Single Cylinder Model for Leg Interference

predict this phenomenon, where a cylinder contains all the geometry of the actuator and at each time the shortest distance between two adjacent cylinders is checked not exceeding the diameter of the cylinder. The model using a single cylinder to represent the whole actuator, is very conservative and will be fail to apply to an actuator whose lower portion may be thicker than the upper portion due to the assembly of position sensor, hydraulic hose, etc., and the locations of top joints are close. In order to overcome this limitation, the actuator is modeled as a combination of two cylinders with different diameters. The cylinder with a larger diameter and a fixed length, represents the thicker geometry while cylinder with small diameter
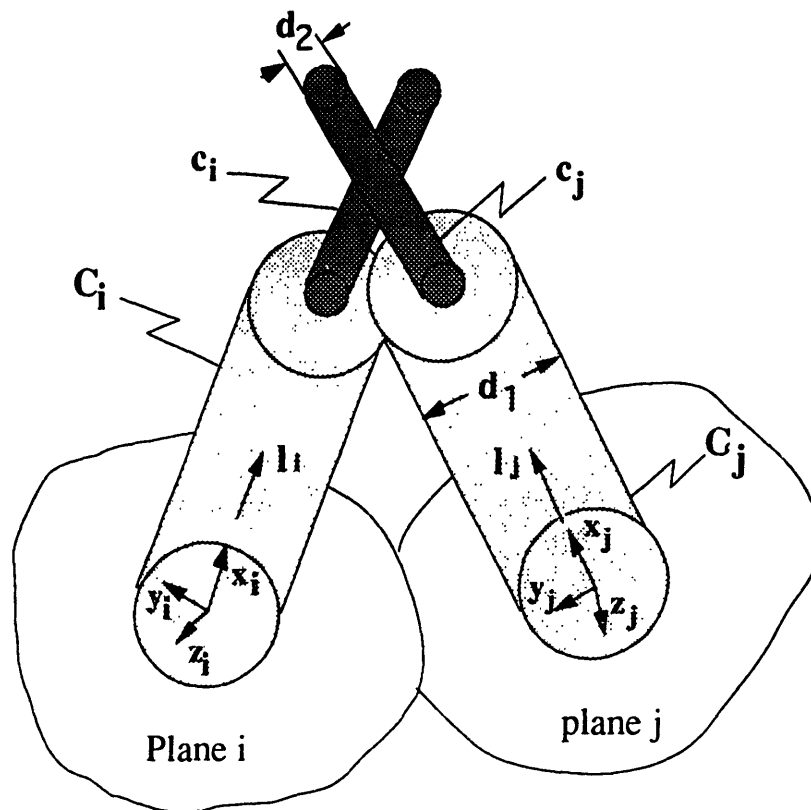
Figure 3.5 Two-Cylinder Model for Leg Interference

and a varying length represents the upper part of the actuator, as shown in Figure 3.5. Now, the leg interference problem becomes the intersection problem between cylinder c_i, C_i, c_j and C_j, ($i, j = 1, 2, \cdots, 6$), where c_i and c_j represent small cylinder i and j, and C_i and C_j represent large cylinder i and j, respectively. If any two cylinders intersect at some point, no matter in which direction to look at them, they must keep contact at that point. Therefore, using model 3 of Stewart platform describing in Chapter 2, we can project all four cylinders into plane $y_i z_i$ and plane $y_j z_j$, respectively. Criterion for interference is that it only occurs when two cylinders interfere at both planes. This method is very effective and efficient if the appropriate local Cartesian coordinates are used, because the interference problem is reduced to just a check of intersection of circles and lines, e.g. in plane $y_i z_i$, the projections of cylinder c_i and C_i are two circles and that of cylinder c_j and C_j are just lines. Although this approach is still conservative, it is much less conservative than the old one and it would solve the leg interference problem more realistically.

CHAPTER 4

GRAPHICAL SIMULATION

An interactive graphical simulation program was developed to contribute to the design of the Stewart platform use as VES and its control algorithm. The simulation program has been performed on Personal IRIS workstation, using Unix operating system and C programming language. Figure 4.1 shows the graphical output and user interface features of the program. The main purposes of the program is to provide interactive graphical simulation as a tool for the visualization of the mechanism, to investigate the effects of geometric configuration on workspace and the specifications of the hydraulic system. In addition to acting as a design tool, the algorithm can also be used for graphical preview of the dynamic behavior of the platform and verifying of the platform controller.

4.1 INTERACTIVE FORMAT

The graphical display consists of multiple windows, such as a projected three-dimensional view of Stewart platform, a text area for data entry from the keyboard, a ruler area showing several analog scales for input and a display of top plate's position, orientation and other kinematic parameters, a message area warning any violation of kinematic constraints including leg lengths, joint angles and leg interference, and a menu column containing 10 buttons for different actions, such as joint angle calculation,

---
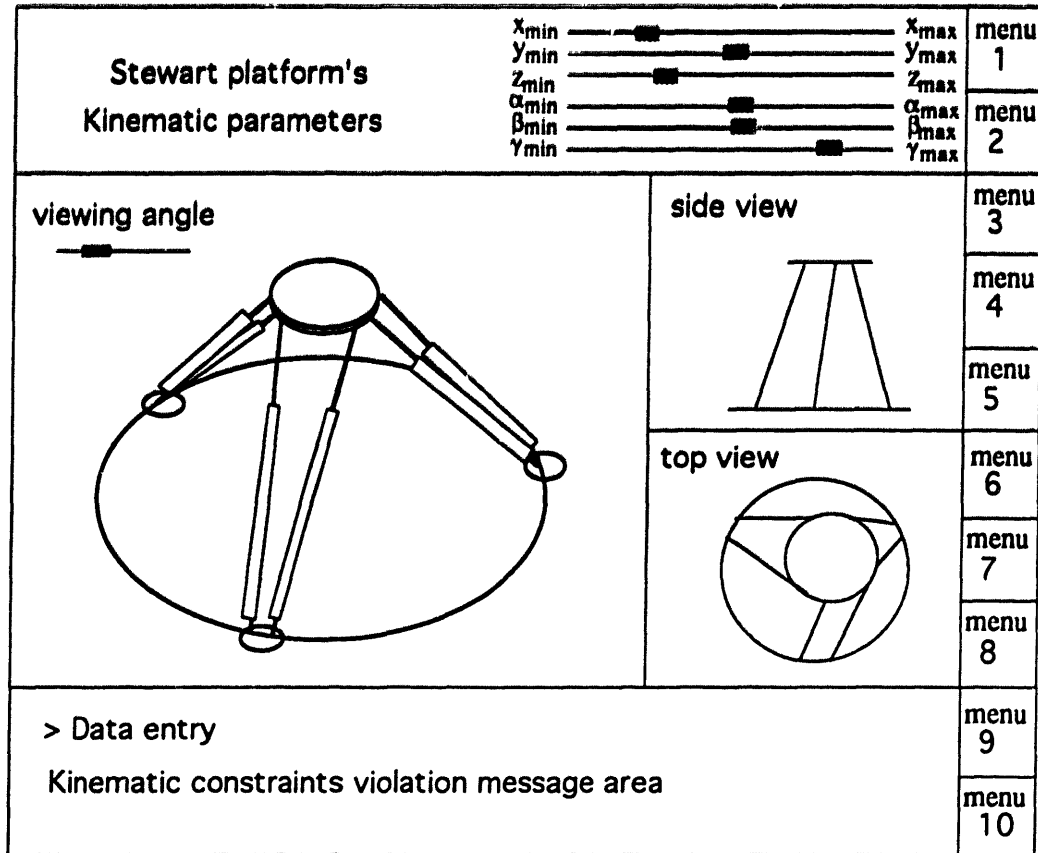
Figure 4.1 Graphical Simulation of Stewart Platform

hydraulic flow rate calculation, coordinate system transformation, etc. The program displays Stewart platform in selected configurations and user controls a mouse to change the viewing angle or the direction in which the platform is projected. For the position or orientation of the platform, user can either input the data from the keyboard or using a mouse to select the analog scale. The orientation can be described using roll, pitch and yaw coordinates or Euler angle coordinates. Alternatively the user can specify a sequence of rotations about the axes fixed to the platform or fixed to the

base. In addition to interactive control of platform position and orientation, the program also provides sinusoidal motion and some other types of motion. The program solve the inverse kinematics to get the leg length, calculate joint angles and the clearance between the legs to check the workspace violation, based on the analysis described in Chapter 2 and 3. Also, the program calculates flow rate of the hydraulic pump according to the amplitude and frequency of platform's motion, which is used to establish the specification of the hydraulic pump and accumulator.

4.2 DESIGN TOOL

Because of the complexity of the geometry of the six-degree-of-freedom Stewart mechanism, there is not a clearly defined optimal design and it is not trivial to check whether or not a proposed design satisfies the design requirements. Therefore, a graphical simulation program is vital to the progress of the design of VES. As a valuable design tool, it provides the visualization of the platform at each point throughout its workspace and variation of the geometry of the platform is investigated graphically until a close to optimal design is achieved. Graphical simulation is used to establish the basic shape of the platform, to check the violation of the kinematic constraints, such as leg length limitations, joint angle limitations and leg interference. The graphical simulation also provides information of the flow rate design parameter which is used to determine the specifications of the hydraulic system of VES.

Table 4.1: Workspace Requirements of VES

Motion	Displacement from Home Position					
	x	y	z	roll	pitch	yaw
Translation	± 12 in	± 12 in	± 12 in			
Rotation				± 30°	± 30°	± 30°

4.2.1 WORKSPACE

The workspace of the Stewart platform is defined as the range of allowable end-effector displacement, i.e. the region of three-dimensional Cartesian space that can be attained by the end-effector with the given orientation of platform of three rotational degrees of freedom. It is determined by the scale and configuration of the mechanism, constrained by the kinematic limitations. The optimal design of Stewart platform is to choose a geometry for which the resulting workspace spans the desired range of motion.

Based on the available laboratory space and the investigation of applications of robot to operate from moving bases or in nonstationary environment, workspace requirements of VES was specified in terms of the amplitude of motion of the platform from its home position in three translational and three rotational degrees of freedom, listed in table 4.1. Here, numerical values are used to define the workspace of the platform,

but in fact the workspace embedded in a six-dimensional space is not a quantity. In recent years, several researchers have addressed the workspace analysis, focus on generating planar graphical contour maps or cross section of the workspace. (Yang and Lee [17], Fichter [11], Weng et al [16], Cwiakala [23], Gosselin [24,25], Clearly and Arai [22])

Graphical simulation program, based on kinematic analysis, provides a qualitative evaluation of the Stewart platform design, and feedback information is then used to modify the design. In order to determine the suitability of a proposed design for specified workspace requirements, the simulation program searches the boundaries of the workspace where at least one of kinematic constraints is violated and checks whether or not the boundary point is within the desired range of motion. The searching is undertaken in all directions and search space is scaled up and down as appropriate. The graphical simulation provides some insight into the shape of the workspace and effects of geometry on the relative amounts of rotational and translational freedom. The simulation program allows the user to interactively specify and change all the design parameters and chose the type of scaling until the most appropriate platform geometry for VES is achieved.

Using the simulation program, a design is found that meets the workspace requirements given the dimensions of readily available mechanical components and the available laboratory space. The resulting geometric parameters and mechanical limitations are listed in table 4.2.

Table 4.2: Platform Geometric Parameters

Platform Geometric Parameters	
Base Radius R	52.77 in
Platform Radius r	12.0 in
Base Angle ϕ_1	3.26°
Platform Angle ϕ_2	14.48°
Angle of Legs to the Base θ	50°
Stroke of Actuator	30.0 in
Kinematic Limitations	
Minimum Actuator Length	22.0 in
Top Joint Angle	45°
Base Joint Angle	45°

Figure 4.2 is an example of the shape of the workspace of the platform, showing the reachable rotational degree of platform before the violation of any kinematic constraints when the platform moves along the vertical direction axis or along the horizontal axis. From the figure, it is seen that the shape of the workspace has some concavities. For the purpose of control, we model the nominal workspace as a convex shape within the real workspace so that any line segment connected by any two points within this space will not go beyond the real workspace of the platform.
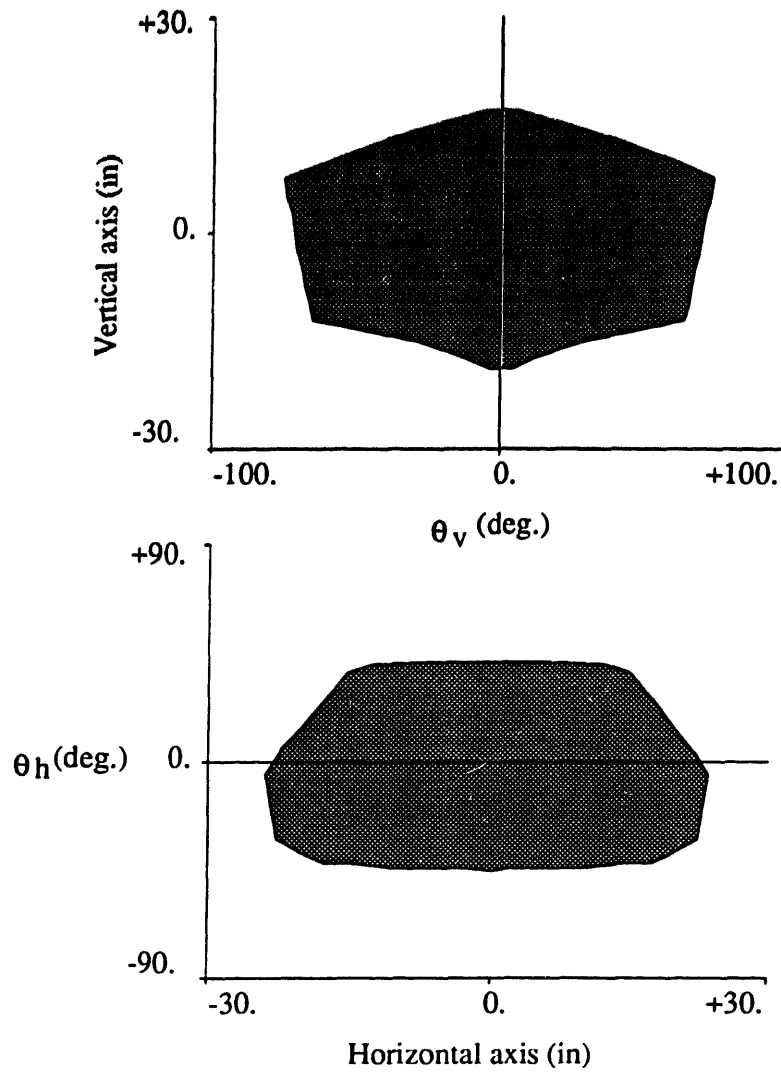
Figure 4.2 Workspace of the Stewart Platform

4.2.2 JOINT ANGLE

Since Stewart platform is a parallel configuration of six adjustable legs connected by universal or spherical joints to the platform and the base, joints play an important role in determining the flexibility and workspace of the platform. Graphical simulation results are very useful in assessing
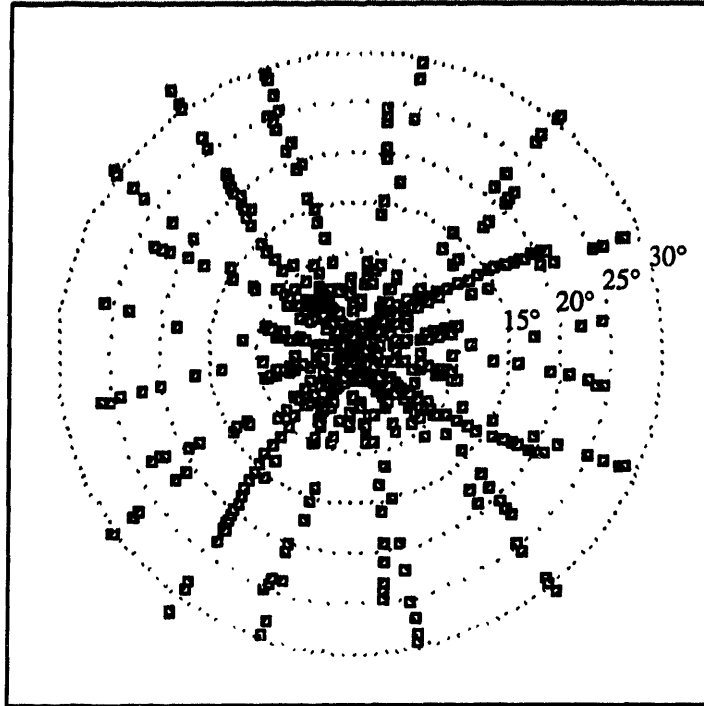
Figure 4.3 The Range of Top joint Angle

the qualitative features of rotational freedom of the joints and the orientation of the joint axes. Figure 4.3 shows a polar plot of the top universal joint angles as the position of the platform is varied throughout its workspace. A point on the plot gives the angle value of the joint by its radius and shows the direction of the rotation by its location. The range of the joints and the angle at which the joints are attached relative to the platform or base are specified using this information. Joints are so designed that they would not restricted the motion of the platform.

4.2.3 FLOW RATE

The kinematic limitation on amplitude and frequency of the platform motion is the flow rate of the hydraulic pump and the size of the accumulator. Graphical simulation program determines the appropriate requirements for a hydraulic system by considering sinusoidal motion of the platform at the specified dynamic limits. For the selected platform geometry, Figure 4.4 shows the hydraulic flow rate for a 0.5 Hz and 12"
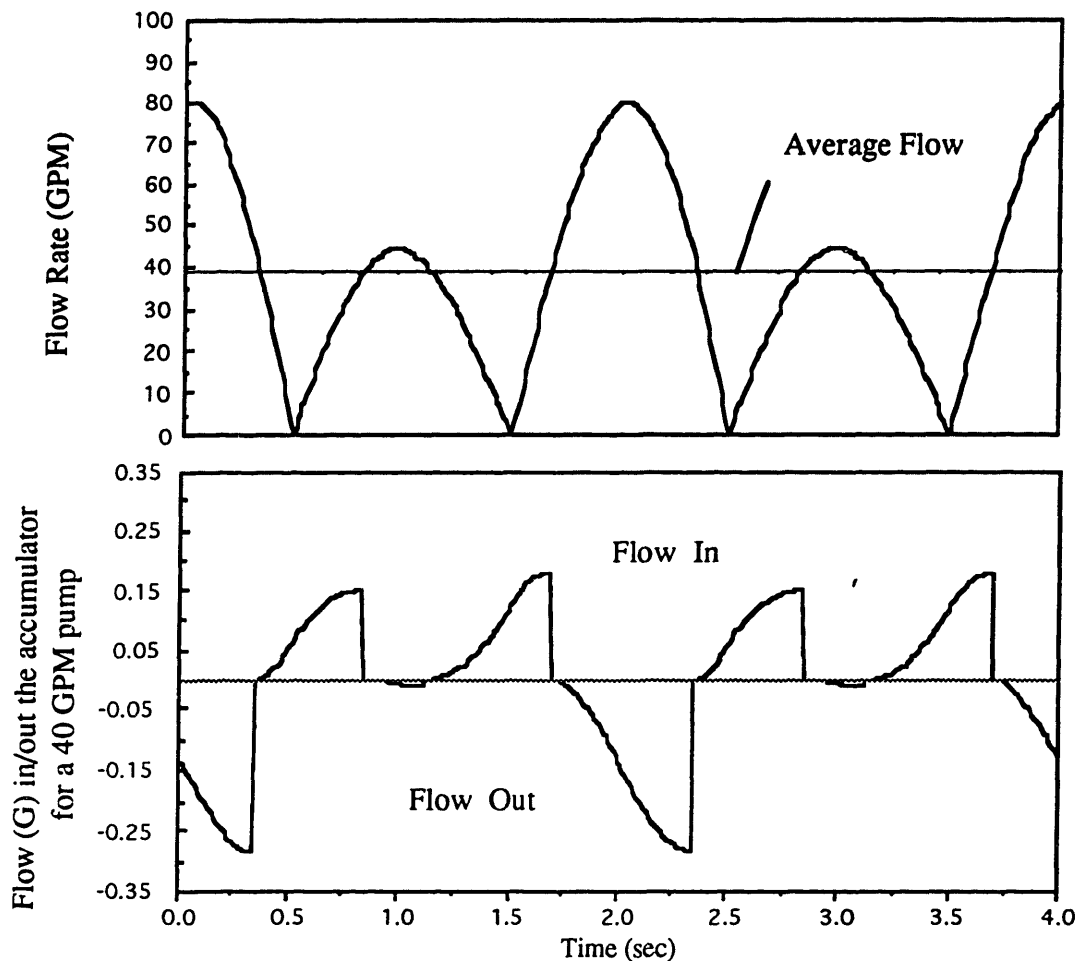
Figure 4.4 Flow Rate of the Hydraulic Pump

amplitude sinusoidal motion in the vertical direction and accumulator flow needed to sustain that flow rate with a 40 GPM pump.

4.3 VALIDATION OF CONTROLLER

In addition to acting as a valuable design tool for Stewart platform use as VES, the graphical simulation is used to validate VES controller algorithm. The simulation program also provides graphical preview of the kinematic and dynamic behavior of the platform and error checking schemes etc before applying them to the real platform.

The capabilities of the graphical simulation program could be extended by introducing some other functions like error compensation, stiffness analysis and dynamic analysis etc. These algorithms could either work independently or in collaboration with other functions of the program so that the whole graphical simulation program becomes efficient, effective, flexible and very powerful. Some parts of graphical simulation algorithm could be directly implemented on VES controller.to control the platform in the laboratory.

CHAPTER 5

KINEMATICS ERROR CORRECTION

The improvement of the accuracy of the simulation of VES is related to two important activities: calibration and compensation. Kinematic calibration concerns the accurate mapping from leg space to end-effector space while compensation is used in platform control to correct position and orientation errors due to the difference between actual and nominal values of platform parameters. Although calibration and compensation techniques for serial type of manipulators and some closed-loop manipulators have been received considerable attention in recent years (Wu et al [33,34], Ahmad [29], Payannet [32], Vuskovic [30], Ziegert and Datseris [35], Hollerbach and Bennett [31]), no analysis of calibration and compensation for Stewart platform has been presented. Since a lot of other error sources in addition to geometric parameters contribute to the inaccuracy of the simulation of VES, such as non-geometric factors like joint compliance and backlash, repeatability of platform, resolution of instrumentation and control structure, error correction for VES will involves theories and techniques in different fields. In order to provide bounds on this topic, error correction problem discussed here is restricted to a static geometric parameters analysis, leaving such non-geometric, time-varying or dynamic effects as backlash, servo and force sensor errors, and platform vibrations to future works.

5.1 ERROR CALIBRATION

The purpose of calibration is to identify the actual values of geometric parameters of the platform. The previous kinematic analysis is based on such an assumption that the Jacobian matrix [J] represents the mapping between leg vector space and end-effector vector space. But, this is only true for ideal model of the platform. For the real platform, variations of geometric parameters such as the locations of joints and the concentricity of the top plate and base arise from imprecision in the manufacturing and assembly process. The real geometric parameters generally deviate from their nominal values. Let vector c represent the real geometric parameters of the platform, whose components are locations of joints, the centers of base and top plate etc, and c_n corresponds to the nominal value of c in the ideal case, we have

$$c = c_n + \Delta c \qquad \text{Eqn. (5.1)}$$

where Δc is the parameter variations. For the real platform, leg length vector is the function of geometric parameter c and the configuration of the platform x, i.e.

$$l = l(c, x) \qquad \text{Eqn. (5.2)}$$

For nominal value of geometric parameter c_n, it becomes

$$l = l(c_n, x) = l_n(x) \qquad \text{Eqn. (5.3)}$$

where l_n represent the nominal leg length vector and it is exact Eqn. (2.19) and corresponding Jacobian matrix is

$$[J] = \left[\frac{\partial l}{\partial x}\right]_{c=c_n} = \left[\frac{\partial l_n}{\partial x}\right]$$

Eqn. (5.4)

which is exact Eqn. (2.22). For the desired end-effector position vector x_d, we have

$$l(c_n, x_d) = l_n(x_d) = l_d$$

Eqn. (5.5)

where l_d is the desired leg length corresponding to x_d at nominal value case. However, for the real platform, due to the deviation of the geometric parameters, the leg length corresponding to the desired end-effector configuration x_d is

$$l = l(c, x_d) \neq l_d$$

Eqn. (5.6)

therefore, even the VES controller is good enough to drive the legs to reach exactly the desired lengths, there still exists an error between the configuration of the platform and the desired configuration, i.e.

$$x = l^{-1}(c, l_d) \neq x_d$$

Eqn. (5.7)

If we assume that error due to the deviations of geometric parameters is

small, global constant and not dependent of configuration of the platform, the desired leg length of the real platform could be written as

$$l_d = l(c, x) = l(c_n + \Delta c, x_d + \Delta x)$$

Eqn. (5.8)

where

$$\Delta x = x - x_d$$

Eqn. (5.9)

is the configuration deviation of the real platform when its leg length is l_d. If we expand Eqn. (5.8) in Taylor series and neglect the higher order terms, we obtain

$$l_d = l(c_n, x_d) + \left[\frac{\partial l}{\partial c}\right]_{\substack{x = x_d \\ c = c_n}} \Delta c + \left[\frac{\partial l}{\partial x}\right]_{\substack{x = x_d \\ c = c_n}} \Delta x$$

Eqn. (5.10)

substitute Eqn. (5.4) and Eqn. (5.5) into the above equation,

$$l_d = l_d + \left[\frac{\partial l_n}{\partial c}\right]_{x = x_d} \Delta c + \left[\frac{\partial l_n}{\partial x}\right]_{x = x_d} \Delta x$$

Eqn. (5.11)

Now, we have a relation between the deviation of the configuration and deviation of geometric parameters.

$$\left[\frac{\partial l_n}{\partial c}\right] \Delta c + [J] \Delta x = 0$$

Eqn. (5.12)

With this relation, we can calibrate the platform to find the exact platform geometric parameters. Eqn. (5.10) could be rewritten as

$$\Delta c = -\left[\frac{\partial l_n}{\partial c}\right]^{-1} [J] \Delta x$$

Eqn. (5.13)

Calibration proceeds by positioning the platform in many configurations within the workspace of the platform or letting the platform follow some known test trajectories. Since we can measure the corresponding leg lengths for each configuration, using the forward kinematics algorithm, discussed in Chapter 4, we can obtain the deviation of configuration Δx and so finally solve for geometric deviation Δc.

There are a number of issues that arise when executing this procedure, which will be related to techniques in different fields. One issue has to do with the measurements of position and orientation of platform as well as the measurements of leg lengths and the advanced instrumentation is required. The effects on the accuracy of the measurement by the error due to noise, drift and nonlinearity should be diminished. Potentially the most serious issue is optimal choice of geometric parameters to be calibrated. The dimension of the vector c or Δc is not restricted. A large dimension vector will increase the possibility of accurate and converging calibration but at the same time increase the difficulty of calculation of matrix $\left[\frac{\partial l_n}{\partial c}\right]$ and its inverse matrix, and the mount of experiment work might be excessive. A small dimension vector

could result in an ill condition for the convergence of the solution or the invertability problem of matrix $\left[\frac{\partial l_n}{\partial c}\right]$, arising from singularities or from data not being "persistently exciting". Since we only deal with the deviation of geometric parameters, how to delete the effects of non-geometric factors such as backlash and joint compliance should be very carefully considered in the experiments. In order to obtain an accurate and stable solution, a parameter identification procedure including the method of statistical approximation must also be applied.

5.2 ERROR COMPENSATION

Two approaches for the compensation of the position and orientation errors due to the variations of geometric parameters are considered.

Method 1: This method is based on the redefinition of the desired position and orientation of the platform before applying the nominal inverse kinematics. The modified desired platform configuration vector x_d^*, which will bring the legs into the correct lengths corresponding to the desired position and orientation of the platform x_d, is

$$x_d^* = x_d + \Delta x_d \qquad \text{Eqn. (5.14)}$$

where

$$\Delta x_d = -[J]^{-1}\left[\frac{\partial l_n}{\partial c}\right]\Delta c \qquad \text{Eqn. (5.15)}$$

This method requires the inversion of the platform Jacobian matrix. Obviously, this approach cannot be applied for the singular configuration or even near singular configuration of the platform, when the Jacobian matrix becomes a singular or near singular matrix.

Method 2: Instead of redefining the position and orientation of the platform, this method directly correct the leg lengths corresponding to the desired configuration of the platform x_d. For small geometric parameters error Δc, the modified leg length is

$$I_d^* = I_d + \Delta I_d \qquad\qquad \text{Eqn. (5.16)}$$

where

$$\Delta I_d = [J]\Delta x = -\left[\frac{\partial I_n}{\partial c}\right]\Delta c \qquad\qquad \text{Eqn. (5.17)}$$

From the analysis in previous section, it is shown that both approaches are equivalent in terms of the compensation effect if the geometric parameter variations are sufficiently small. However, the second method does not require computation of the inverse Jacobian matrix and thus can be used in the singular configurations of the platform. In addition, this method is superior in terms of time efficiency.

CHAPTER 6

CONCLUSION AND RECOMMENDATIONS

The design process of a six-degree-of-freedom, parallel linked, hydraulic driven Stewart platform use as Vehicle Emulator System is thoroughly discussed.

Two additional design considerations were proposed: stiffness and admittance emulation accuracy. Detail analyses reveal the relationship between the simulation error, components of Vehicle Emulation System and performance specifications of VES. Analysis results show the dominant factors which affect the performance of VES in static case, space simulation case and vehicle simulation case, therefore, they provide insight and some guidelines to the design process of Stewart platform.

Different kinematic models of the platform were discussed and compared. A new approach for numerically solving the forward kinematics was presented. In contrast to other numerical methods, it is more efficient because of not requiring the calculation of 6×6 inverse Jacobian matrix and it is also remediable when the configuration is in the singular state. Kinematic constraints of the platform are analyzed and a new algorithm was developed so that the leg interference problem could be solved more realistically.

A graphical simulation program based on analysis was developed and used as a valuable design tool to investigate the effects of geometry and constraints on the motion of the Stewart platform and to provide the useful information about workspace, joint angle and hydraulic flow rate. The simulation program allows the user to explore the different design alternatives by interactively specifying and changing the design parameters until a close to optimal design which satisfies all the design requirements is achieved. The graphical simulation program is also used to preview the experiment, to check the software error and to validate the control algorithm.

The approach for correcting the position and orientation error of Stewart platform due to the variations of geometric parameters was discussed. The analytical formulas for improving the tracking accuracy either by modifying desired leg length or modifying the desired position and orientation of the platform were given.

Future work to improve the design of Stewart platform used as VES should include the development of a six-degree-of-freedom dynamic model of Stewart platform which could be used in accuracy analysis, impedance (dynamic stiffness) analysis and advanced VES controller. Forward kinematics of Stewart platform is a good research topic, which is not only of theoretical importance, and also practically critical for error calibration, failure recovery and dynamic simulation. In order to obtain a good, accurate VES simulation , we have to thoroughly study a lot of issues

concerning error compensation for Stewart platform, such as error effects due to backlash of joints, servo and force sensor errors, and platform vibrations etc.

APPENDIX

Appendix 1.1

The follwing figure shows a one-degree-of-freedom translation model of VES. The robot and platform move only along the vertical direction. me is the mass of the robot and m is the mass of the base to be simulated.
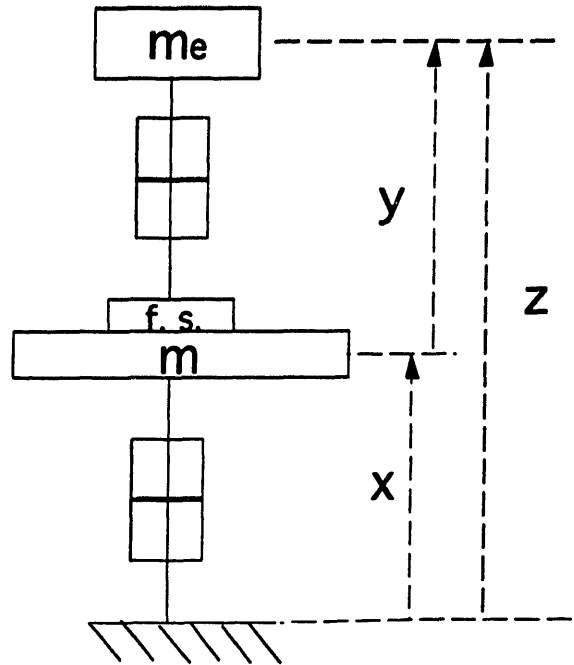
$z = x+y$ $m_e\ddot{z} = f$ $\therefore m_e(\ddot{x}+\ddot{y}) = f$

since $f_s = -f$ $\therefore m\ddot{x} = f_s = -f$

$\therefore m_e(\ddot{x}+\ddot{y}) = -m\ddot{x}$, or $(m_e+m)\ddot{x} = -m_e\ddot{y}$

If we assume the motion of robot is a typical sinusoidal motion, $y = Y\sin\omega t$, where Y is the magnitude of robot motion and ω is the frequency of robot motion, we have

$\dot{y} = Y\omega\cos\omega t$ and $\ddot{y} = -Y\omega^2\sin\omega t = -\omega^2 y$

We also assume zero initial conditions, i.e.,

$x = 0, \dot{x} = 0, y = 0, \dot{y} = 0$ when $t = 0$.

$$\therefore \quad x = -\frac{m_e}{m+m_e}y \quad \text{and} \quad z = x+y = -\frac{m_e}{m+m_e}y + y = \frac{m}{m+m_e}y$$

(i) Due to the offset error of the force sensor $\Delta f_o = \beta f_{smax} = \beta m \ddot{x}_{max}$, and from the equation $m(\Delta \ddot{x}) = \Delta f_o = \beta m \ddot{x}_{max} = -\beta \frac{m m_e}{m+m_e}\ddot{y}_{max}$, we integrate twice and get

$$\Delta x|_{\Delta f_o} = \beta \frac{m_e}{m+m_e}Y\omega^2 t^2$$

Since VES uses admittance model, the Δx won't affect y, i.e., $\Delta y|_{\Delta f_o} = 0$

$$\therefore \quad \Delta z|_{\Delta f_o} = \Delta x|_{\Delta f_o} + \Delta y|_{\Delta f_o} = \beta \frac{m_e}{m+m_e}Y\omega^2 t^2$$

and also we have $z_{max} = \frac{m}{m+m_e}Y$, so, the error of simulation due to offset error of the force sensor is

$$\varepsilon_o = \frac{|\Delta z|}{|z_{max}|} = \beta \frac{m_e}{m}\omega^2 t^2$$

(ii) Due to the gain error of the force sensor $\Delta f_g = \gamma f_s = -\gamma f = \gamma m \ddot{x} = -\gamma \frac{m m_e}{m+m_e}\ddot{y}$, and from the equation $m(\Delta \ddot{x}) = \Delta f_g = \gamma m \ddot{x}$, integration gives us

$$\Delta x|_{\Delta f_g} = -\gamma \frac{m_e}{m+m_e}y = \gamma x$$

therefore, the error of simulation due to gain error of the force sensor is

$$\varepsilon_g = \frac{\Delta z|_{\Delta f_g}}{z} = \frac{\Delta x|_{\Delta f_g}}{z} = \frac{\frac{-\gamma m_e}{m+m_e}y}{\frac{m}{m+m_e}y} = -\gamma \frac{m_e}{m}$$

$$J_e = m_e l^2$$

$$J = mr_g^2$$

A
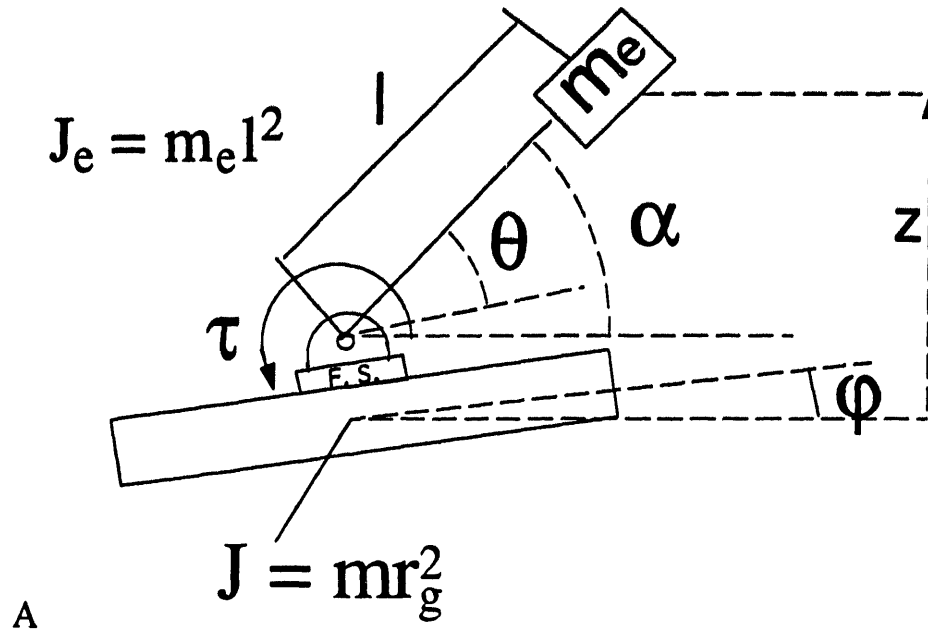
If we modify the one-degree-of-freedom model as shown in Appendix1.1 to analyze VES rotational motion, and consider robot motion $\theta = \Theta \sin \omega t$, we have

$$\alpha = \theta + \varphi , \quad J_e \ddot{\alpha} = m_e l^2 \ddot{\alpha} = \tau, \quad \therefore m_e l^2 (\ddot{\theta} + \ddot{\varphi}) = \tau, \quad \text{since } \tau_s = -\tau$$

$$\therefore J \ddot{\varphi} = mr_g^2 \ddot{\varphi} = \tau_s = -\tau$$

$$(m_e l^2 + mr_g^2) \ddot{\varphi} = -m_e l^2 \ddot{\theta}$$

$$\dot{\theta} = \Theta \omega \cos \omega t \quad \text{and} \quad \ddot{\theta} = -\Theta \omega^2 \sin \omega t = -\omega^2 \theta$$

We assume zero initial conditions, i.e.,

$$\theta = 0, \ \dot{\theta} = 0, \ \varphi = 0, \ \dot{\varphi} = 0 \quad \text{when } t = 0$$

$$\therefore \quad \varphi = -\frac{J_e}{J_e + J} \theta = -\frac{m_e l^2}{m_e l^2 + mr_g^2} \theta$$

$$\alpha = \phi + \theta = \frac{J}{J_e + J}\theta = \frac{mr_g^2}{m_e l^2 + mr_g^2}\theta$$

(i) Due to the offset error of the force sensor $\Delta f_o = \beta \tau_{smax} = \beta J \ddot{\phi}_{max}$, and from

the equation $J(\Delta \ddot{\phi}) = \Delta f_o = \beta J \ddot{\tau}_{smax} = -\beta \frac{JJ_e}{J + J_e} \ddot{\theta}_{max}$, we integrate twice and get

$$\Delta \phi|_{\Delta f_o} = \beta \frac{J_e}{J + J_e} \Theta \omega^2 t^2$$

since $\Delta \theta|_{\Delta f_o} = 0$

$$\therefore \quad \Delta \alpha|_{\Delta f_o} = \Delta \phi|_{\Delta f_o} = \beta \frac{J_e}{J + J_e} \Theta \omega^2 t^2 = \beta \frac{m_e l^2}{mr_g^2 + m_e l^2} \Theta \omega^2 t^2$$

and also we have $\alpha_{max} = \frac{J}{J + J_e}\Theta$, therefor, the error of simulation due to offset error of the force sensor is

$$\varepsilon_o = \frac{|\Delta \alpha|}{|\alpha_{max}|} = \beta \frac{J_e}{J} \omega^2 t^2 = \beta \frac{m_e}{m}(\frac{1}{r_g})^2 \omega^2 t^2$$

(ii) Due to the gain error of the force sensor $\Delta f_g = \gamma \tau_s = -\gamma \tau = \gamma J \ddot{\phi} = -\gamma \frac{JJ_e}{J + J_e}\ddot{\theta}$,

and from the equation $J(\Delta \ddot{\phi}) = \Delta f_g = \gamma J \ddot{\phi}$, integration gives us

$$\Delta \phi|_{\Delta f_g} = \gamma \phi = -\frac{\gamma J_e}{J_e + J}\theta = -\frac{\gamma m_e l^2}{m_e l^2 + mr_g^2}\theta$$

$$\Delta \alpha|_{\Delta f_g} = \Delta \phi|_{\Delta f_g} + \Delta \theta|_{\Delta f_g} = \Delta \phi|_{\Delta f_g} + 0 = \Delta \phi|_{\Delta f_g}$$

so, the error of simulation due to gain error of the force sensor is

$$\varepsilon_g = \frac{\Delta \alpha}{\alpha} = -\gamma \frac{J_e \theta /(J_e + J)}{J\theta /(J_e + J)} = -\gamma \frac{J_e}{J} = -\gamma \frac{m_e}{m}(\frac{1}{r_g})^2$$

Appendix 1.3

Combining two one-degree-of-freedom models, which are discussed in Appendix1.1 and 1.2, we can develop a simple two-degrees-of-freedom model. The robot motion is still a prue sinusoidal rotation, but the base can move vertically or rotate corresponding to the force or torque the force sensor measuires. In order to simplify the analysis, small motion of the base system is assumed and the cross-talk effect between force sensor channels is not considered.
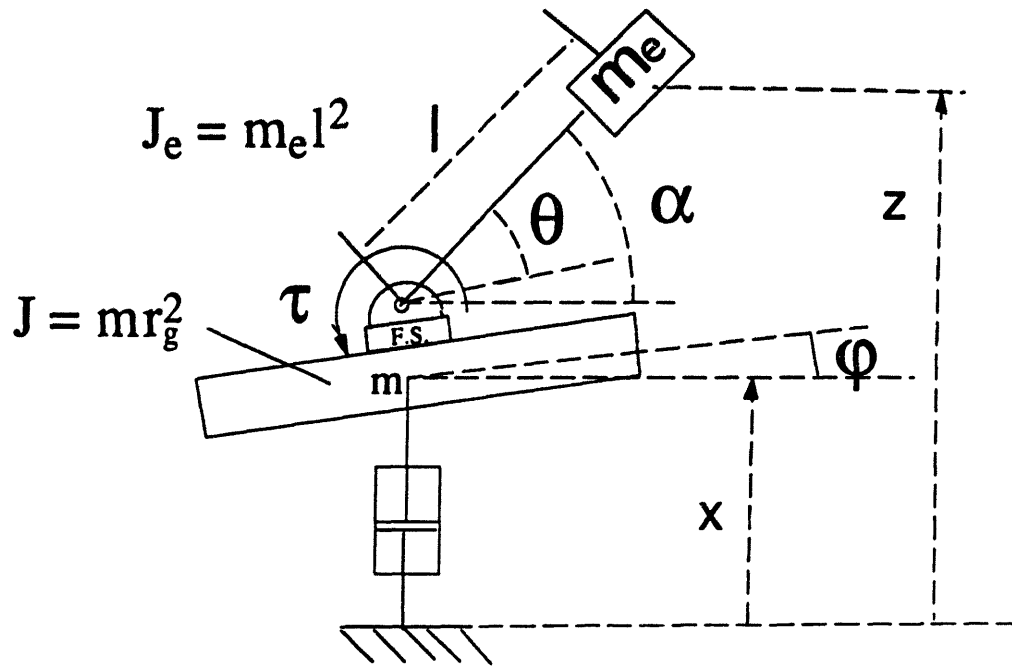
$$\alpha = \theta + \varphi \qquad z = x + l\alpha \qquad J_e\ddot{\alpha} = m_e l^2 \ddot{\alpha} = \tau \qquad \therefore \ m_e l^2 (\ddot{\theta} + \ddot{\varphi}) = \tau$$

for the base system,

$$m\ddot{x} = f_s \qquad J\ddot{\varphi} = mr_g^2\ddot{\varphi} = \tau_s$$

since $\tau_s = -\tau$ and $f_s = -m_e\ddot{z} = -m_e(\ddot{x} + l\ddot{\alpha})$

$$\therefore \ (m_e l^2 + mr_g^2)\ddot{\varphi} = -m_e l^2 \ddot{\theta} \qquad \text{and} \qquad (m + m_e)\ddot{x} = -m_e l\ddot{\alpha}$$

Assuming zero initial conditions, integration gives us

$$\varphi = -\frac{J_e}{J_e + J}\theta = -\frac{m_e l^2}{(m_e l^2 + mr_g^2)}\theta$$

$$\therefore \quad \alpha = \theta + \varphi = \frac{J}{J_e + J}\theta = \frac{mr_g^2}{m_e l^2 + mr_g^2}\theta$$

and also

$$x = -\frac{m_e l}{m + m_e}\alpha = \frac{-(m_e l)(mr_g^2)}{(m + m_e)(m_e l^2 + mr_g^2)}\theta$$

Check the solution. Since initial conditions are all zero, the center of the system must remain zero, i.e.,

$$z_c \equiv 0 \quad \text{or} \quad \sum_i m_i z_i \equiv 0 \quad \text{i.e.} \quad m_e z + mx = 0$$

$$\text{since} \quad z = x + l\alpha = -\frac{m_e l}{m + m_e}\alpha + l\alpha = \frac{ml}{m + m_e}\alpha$$

$$\therefore \quad m_e z = m_e(x + l\alpha) = \frac{m_e m}{m + m_e}l\alpha$$

$$mx = m(-\frac{m_e l\alpha}{m + m_e}) = -m_e z$$

$$\therefore \quad m_e z + mx \equiv 0$$

(i)Assuming offset error of the force sensor is

$$\Delta f_o = \begin{Bmatrix} \Delta f_o \\ \Delta \tau_o \end{Bmatrix} = \beta \begin{Bmatrix} f_{smax} \\ \tau_{smax} \end{Bmatrix}$$

Integrating the equation

$$J\Delta\ddot{\varphi} = \Delta\tau_o = \beta\tau_{smax} = \beta J\ddot{\varphi}_{max} = -\beta\frac{J J_e}{J_e + J}\ddot{\theta}_{max} = \beta\frac{J J_e}{J_e + J}\omega^2\Theta$$

and assuming zero initial conditions, we get

$$\Delta\varphi|_{\Delta f_o} = \beta \frac{J_e}{J+J_e} \Theta \omega^2 t^2$$

since $\Delta\theta|_{\Delta f_o} = 0$

$$\therefore \quad \Delta\alpha|_{\Delta f_o} = \Delta\varphi|_{\Delta f_o} = \beta \frac{J_e}{J+J_e} \Theta \omega^2 t^2 = \beta \frac{m_e l^2}{mr_g^2 + m_e l^2} \Theta \omega^2 t^2$$

Assuming zero initial conditions and integrating the following equation

$$m\Delta\ddot{x} = \Delta f_o = \beta f_{smax} = \beta m\ddot{x}_{max} = -\beta \frac{m \, m_e l}{m_e + m} \ddot{\alpha}_{max} = \beta \frac{m \, m_e l}{(m_e + m)(J_e + J)} \omega^2 \Theta$$

$$\therefore \quad \Delta x|_{\Delta f_o} = \beta \frac{m_e l}{(m_e + m)(J_e + J)} J\Theta \omega^2 t^2$$

so, we have

$$\Delta z|_{\Delta f_o} = \Delta x|_{\Delta f_o} + l\Delta\alpha|_{\Delta f_o} = \beta \frac{m_e l}{(m_e + m)(J_e + J)} J\Theta \omega^2 t^2 + \beta \frac{J_e l\Theta}{(J_e + J)} \omega^2 t^2$$

$$= \beta\omega^2 t^2 \frac{\Theta m_e l}{(J_e + J)} [\frac{J}{(m_e + m)} + l^2]$$

and also we have

$$z_{max} = \frac{ml}{m + m_e} \alpha_{max} = \frac{ml}{m + m_e} \frac{J}{J + J_e} \Theta$$

so, the error of simulation due to offset error of the force sensor is

$$\varepsilon_o = \frac{|\Delta z|}{|z_{max}|} = \beta\omega^2 t^2 m_e l \frac{m_e + m}{mlJ} [\frac{J}{m_e + m} + l^2]$$

$$= \beta\omega^2 t^2 \frac{m_e}{m} [1 + \frac{m_e + m}{mr_g^2} l^2] = \beta\omega^2 t^2 \frac{m_e}{m} [1 + (\frac{l}{r_g})^2 + \frac{m_e}{m}(\frac{l}{r_g})^2]$$

ii)Assuming gain error of the force sensor is

$$\Delta f_g = \begin{Bmatrix} \Delta f_g \\ \Delta \tau_g \end{Bmatrix} = \gamma \begin{Bmatrix} f_s \\ \tau_s \end{Bmatrix}$$

Integrating the equation

$$J\Delta\ddot{\varphi} = \Delta\tau_g = \gamma\tau_s = \gamma J\ddot{\varphi} = -\gamma\frac{J\,J_e}{J_e+J}\ddot{\theta}$$

and assuming zero initial conditions, we get

$$\Delta\varphi|_{\Delta f_s} = \gamma\varphi = -\gamma\frac{J_e}{J+J_e}\theta$$

since $\Delta\theta|_{\Delta f_s} = 0$

$$\therefore \quad \Delta\alpha|_{\Delta f_s} = \Delta\varphi|_{\Delta f_s} = -\gamma\frac{J_e}{J+J_e}\theta$$

Assuming zero initial conditions and integrating the following equation

$$m\Delta\ddot{x} = \Delta f_g = \gamma f_s = \gamma m\ddot{x} = -\gamma\frac{m\,m_e l}{m_e+m}\ddot{\alpha} = -\gamma\frac{m\,m_e l}{(m_e+m)\,(J_e+J)}J\ddot{\theta}$$

$$\therefore \quad \Delta x|_{\Delta f_s} = -\gamma\frac{m_e l}{(m_e+m)\,(J_e+J)}J\theta$$

so, we have

$$\Delta z|_{\Delta f_s} = \Delta x|_{\Delta f_s} + l\Delta\alpha|_{\Delta f_s} = -\gamma\frac{m_e l}{(m_e+m)\,(J_e+J)}J\theta - \gamma\frac{J_e l}{(J_e+J)}\theta$$

$$= -\gamma\frac{\theta m_e l}{(J_e+J)}[\frac{J}{(m_e+m)} + l^2]$$

and also we have $\quad z = \frac{ml}{m+m_e}\alpha = \frac{ml}{m+m_e}\frac{J}{J+J_e}\theta$

therefore, the error of simulation due to gain error of the force sensor is

$$\varepsilon_g = \frac{\Delta z}{z} = -\gamma\frac{m_e}{m}\frac{m_e+m}{J}[\frac{J}{m_e+m} + l^2] = -\gamma\frac{m_e}{m}[1 + \frac{m_e+m}{mr_g^2}l^2]$$

$$= -\gamma\frac{m_e}{m}[1 + (\frac{l}{r_g})^2 + \frac{m_e}{m}(\frac{l}{r_g})^2]$$

Appendix 1.4

For VES to simulate more general base system, e.g., the suspension system of a vehicle, the stiffness of the base system is a very important fact, so, it should be considered in the base model in addition to the inertial effect of the base. On the basis of simple two-degrees-of-freedom model, which is discussed in Appendix 1.3, we include stiffness of base system and establish a two-degrees-of-freedom VES model. In the model, the stiffness of the base system includes both translational stiffness k and rotational stiffness kr. Since stiffness exists in the base system, the base will produce a restoring force to balance the error force caused by the offset error of the force sensor. Therefore, in vehicle emulation case, the offset error is static and negligible and the gain error will dominate.

$$J_e = m_e l^2$$

$$J = m r_g^2$$
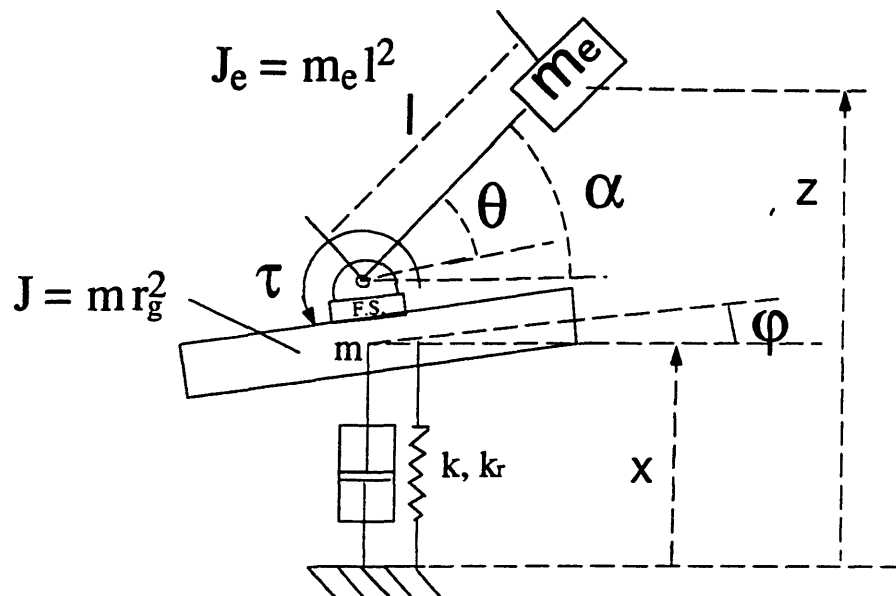
$$\alpha = \theta + \varphi \qquad z = x + l\alpha \qquad J_e \ddot{\alpha} = m_e l^2 \ddot{\alpha} = \tau \qquad \therefore \ m_e l^2 (\ddot{\theta} + \ddot{\varphi}) = \tau$$

for the base system,

$$m\ddot{x} + kx = f_s = -f = -m_e \ddot{z} = -m_e(\ddot{x} + l\ddot{\alpha}) \qquad J\ddot{\varphi} + k_r\varphi = mr_g^2\ddot{\varphi} + k_r\varphi = \tau_s = -\tau$$

$$\therefore \ (J_e + J)\ddot{\varphi} + k_r\varphi = -J_e\ddot{\theta} \qquad or \qquad (m_e l^2 + mr_g^2)\ddot{\varphi} + k_r\varphi = -m_e l^2 \ddot{\theta}$$

and $(m + m_e)\ddot{x} + kx = -m_e l\ddot{\alpha}$

Assuming zero initial conditions and sinusoidal motion of the robot

$\theta = \Theta \sin\omega t$ and $\ddot{\theta} = -\omega^2 \Theta \sin\omega t$

the forced response of the system is

$$\varphi = \frac{\omega^2 J_e}{k_r - (J_e + J)\omega^2}\theta$$

Define

$$\omega_{nr}^2 = \frac{k_r}{(J_e + J)} = \frac{k_r}{(m_e l^2 + mr_g^2)} \quad and \quad M_r = \frac{\omega^2}{\omega^2 - \omega_{nr}^2} = \frac{1}{1 - (\frac{\omega_{nr}}{\omega})^2}$$

$$\therefore \ \varphi = -\frac{M_r J_e}{(J_e + J)}\theta$$

$$\therefore \ \alpha = \theta + \varphi = \frac{J + (1 - M_r)J_e}{J_e + J}\theta$$

Similar, the forced response of x is

$$x = \frac{m_e l\omega^2}{k - (m + m_e)}\alpha = \frac{m_e l\omega^2}{k - (m + m_e)}[\frac{J + (1 - M_r)J_e}{(J_e + J)}]\theta$$

Define

$$\omega_n^2 = \frac{k_r}{(m_e + m)} \quad and \quad M = \frac{\omega^2}{\omega^2 - \omega_n^2} = \frac{1}{1 - (\frac{\omega_n}{\omega})^2}$$

$$\therefore \quad x = -\frac{Mm_el}{(m+m_e)}[\frac{J+(1-M_r)J_e}{(J_e+J)}]\theta$$

Assuming gain error of the force sensor is

$$\Delta f_g = \begin{Bmatrix} \Delta f_g \\ \Delta \tau_g \end{Bmatrix} = \gamma \begin{Bmatrix} f_s \\ \tau_s \end{Bmatrix}$$

$$\therefore \quad \begin{Bmatrix} \Delta x \\ \Delta \varphi \end{Bmatrix} = \gamma \begin{Bmatrix} x \\ \varphi \end{Bmatrix} = -\gamma\theta \begin{Bmatrix} \frac{Mm_el}{(m_e+m)}[\frac{J+(1-M_r)J_e}{(J_e+J)}] \\ \frac{M_rJ_e}{(J_e+J)} \end{Bmatrix}$$

Since $\Delta\theta = 0$

$$\therefore \quad \Delta\alpha = \Delta\theta + \Delta\varphi = \Delta\varphi$$

$$\therefore \quad \Delta z = \Delta x + l\Delta\alpha = -\gamma\theta\frac{Mm_el}{(m_e+m)}[\frac{J+(1-M_r)J_e}{(J_e+J)}] - \gamma\theta l\frac{M_rJ_e}{(J_e+J)}$$

$$= -\frac{\gamma\theta m_el}{(J_e+J)}\{\frac{M}{(m_e+m)}[J+(1-M_r)J_e] + M_rl^2\}$$

and $z = x+l\alpha = -\theta\frac{Mm_el}{(m_e+m)}[\frac{J+(1-M_r)J_e}{(J_e+J)}] + l\theta\frac{J+(1-M_r)J_e}{(J_e+J)}$

$$= \frac{\theta l}{(J_e+J)}[J+(1-M_r)J_e][1-\frac{Mm_e}{(m_e+m)}] = \frac{\theta l}{(J_e+J)}[J+(1-M_r)J_e][\frac{m+(1-M)m_e}{(m_e+m)}]$$

Therefore, the error of simulation due to the gain error of force sensor is

$$\therefore \quad \varepsilon_g = \frac{\Delta z}{z} = \frac{-\frac{\gamma\theta m_el}{(J_e+J)}\{\frac{M}{(m_e+m)}[J+(1-M_r)J_e]+M_rl^2\}}{\frac{\theta l}{(J_e+J)}[J+(1-M_r)J_e][\frac{m+(1-M)m_e}{(m_e+m)}]}$$

$$= \frac{-\gamma m_e\{M[J+(1-M_r)J_e]+(m_e+m)M_rl^2\}}{[J+(1-M_r)J_e][m+(1-M)m_e]}$$

$$= -\gamma\{\frac{Mm_e}{m+(1-M)m_e} + \frac{M_rm_el^2}{[J+(1-M_r)J_e]} + \frac{Mm_eM_rm_el^2}{[J+(1-M_r)J_e][m+(1-M)m_e]}\}$$

Let's discuss some special cases.

(1) $k = 0$ and $k_r = 0$, so $\omega_n = 0$, $\omega_{nr} = 0$, $M = 1$ and $M_r = 1$

$$\therefore \quad \varepsilon_g = \frac{\Delta z}{z} = -\gamma[\frac{m_e}{m} + \frac{m_e}{m}(\frac{l}{r_g})^2 + (\frac{m_e l}{mr_g})^2]$$

This is the same result as that we obtained from simple two-degrees-of-freedom model.

2) $k = 0$ and $k_r \to \infty$, so $\omega_n = 0$, $\omega_{nr} \to \infty$, $M = 1$ and $M_r \to 0$

$$\therefore \quad \varepsilon_g = \frac{\Delta z}{z} \to -\gamma\frac{m_e}{m}$$

This is the same result as that we obtained from simple one-degree-of-freedom translation model. Very large rotational stiffness prevents the base sytem from rotating.

3) $k_r = 0$ and $k \to \infty$, so $\omega_{nr} = 0$, $\omega_n \to \infty$, $M_r = 1$ and $M \to 0$

$$\therefore \quad \varepsilon_g = \frac{\Delta z}{z} \to -\gamma\frac{m_e l^2}{mr_g^2}$$

This is the same result as that we obtained from simple one-degree-of-freedom rotation model. Very large translational stiffness prevents the base sytem from moving.vertically.

(4) For a practical case, when $\omega \ll \omega_n$ and $\omega \ll \omega_{nr}$, we have

$$M \to -\frac{\omega^2}{\omega_n^2} \quad \text{and} \quad 1-M \to 1+\frac{\omega^2}{\omega_n^2} \to 1$$

$$M_r \to -\frac{\omega^2}{\omega_{nr}^2} \quad \text{and} \quad 1-M_r \to 1+\frac{\omega^2}{\omega_{nr}^2} \to 1$$

so the emulation error will approach to

$$\varepsilon_g = \frac{\Delta z}{z} = -\gamma m_e \omega^2[\frac{-1}{k} - \frac{l^2}{k_r} + \frac{m_e l^2 \omega^2}{kk_r}]$$

Appendix 2.1
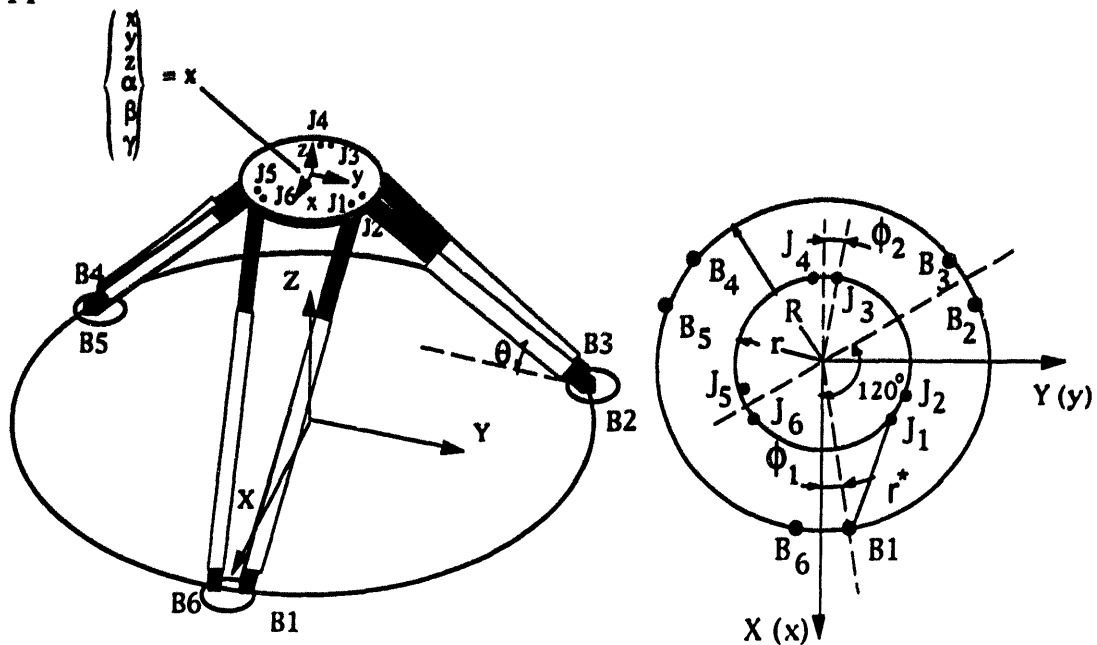
$$x_{J1} = r\sin(\pi/6 + \varphi2);$$
$$x_{J2} = r\sin(\pi/6 - \varphi2);$$
$$x_{J3} = -r\cos(\varphi2);$$
$$x_{J4} = x_{J3};$$
$$x_{J5} = x_{J2};$$
$$x_{J6} = x_{J1};$$

$$y_{J1} = r\cos(\pi/6 + \varphi2);$$
$$y_{J2} = r\cos(\pi/6 - \varphi2);$$
$$y_{J3} = r\sin(\varphi2);$$
$$y_{J4} = -y_{J3};$$
$$y_{J5} = -y_{J2};$$
$$y_{J6} = -y_{J1};$$

$$X_{B1} = R\cos(\varphi1);$$
$$X_{B2} = -R\sin(\pi/6 - \varphi1);$$
$$X_{B3} = -R\sin(\pi/6 + \varphi1);$$
$$X_{B4} = X_{B3};$$
$$X_{B5} = X_{B2};$$
$$X_{B6} = X_{B1};$$

$$Y_{B1} = R\sin(\varphi1);$$
$$Y_{B2} = R\cos(\pi/6 - \varphi1);$$
$$Y_{B3} = R\cos(\pi/6 + \varphi1);$$
$$Y_{B4} = -Y_{B3};$$
$$Y_{B5} = -Y_{B2};$$
$$Y_{B6} = -Y_{B1};$$

Let $x_i^* = x_{Ji} - X_{Bi}$ and $y_i^* = y_{Ji} - Y_{Bi}$, $i = 1, \ldots 6.$, and denote

$s() = \sin()$; $c() = \cos()$; $s^2() = \sin^2()$ and $c^2() = \cos^2()$ etc.

---

since $x_{J1}+x_{J2}+x_{J3} = rs(\pi/6+\varphi 2)+rs(\pi/6-\varphi 2)-rc(\varphi 2)$

$$= r[s(\pi/6)c(\varphi 2)+c(\pi/6)s(\varphi 2)+s(\pi/6)c(\varphi 2)-c(\pi/6)s(\varphi 2)-c(\varphi 2)]$$

$$= r[0.5c(\varphi 2)+0.5c(\varphi 2)-c(\varphi 2)]= 0$$

so $\displaystyle\sum_{i=1}^{6} x_{Ji}=x_{J1}+x_{J2}+x_{J3}+x_{J4}+x_{J5}+x_{J6}=x_{J1}+x_{J2}+x_{J3}+(x_{J3}+x_{J2}+x_{J1})$

$$=2(x_{J1}+x_{J2}+x_{J3}) = 0$$

since $X_{B1}+X_{B2}+X_{B3} = Rc(\varphi 1)-Rs(\pi/6-\varphi 1)-Rs(\pi/6+\varphi 1)$

$$= R[c(\varphi 1)-s(\pi/6)c(\varphi 1)+c(\pi/6)s(\varphi 1)-s(\pi/6)c(\varphi 1)-c(\pi/6)s(\varphi 1)]$$

$$= R[c(\varphi_1)-0.5c(\varphi 1)-0.5c(\varphi 1)]= 0$$

so

$$\sum_{i=1}^{6} X_{Bi}=X_{B1}+X_{B2}+X_{B3}+X_{B4}+X_{B5}+X_{B6}=(X_{B1}+X_{B2}+X_{B3})+(X_{B3}+X_{B2}+X_{B1})$$

$$=2(X_{B1}+X_{B2}+X_{B3}) = 0$$

$$\sum_{i=1}^{6} y_{Ji}=y_{J1}+y_{J2}+y_{J3}+y_{J4}+y_{J5}+y_{J6}=(y_{J1}+y_{J2}+y_{J3})+(-y_{J3}-y_{J2}-y_{J1})= 0$$

$$\sum_{i=1}^{6} Y_{Bi}=Y_{B1}+Y_{B2}+Y_{B3}+Y_{B4}+Y_{B5}+Y_{B6}$$

$$=(Y_{B1}+Y_{B2}+Y_{B3})+(-Y_{B3}-Y_{B2}-Y_{B1})=0$$

$$\sum_{i=1}^{6} x_i^{*}= \sum_{i=1}^{6} (x_{Ji}-X_{Bi}) = \sum_{i=1}^{6} x_{Ji}-\sum_{i=1}^{6} X_{Bi} = 0$$

$$\sum_{i=1}^{6} y_i^* = \sum_{i=1}^{6} (y_{Ji} - Y_{Bi}) = \sum_{i=1}^{6} y_{Ji} - \sum_{i=1}^{6} Y_{Bi} = 0$$

$$\sum_{i=1}^{6} x_i^* y_i^* = x_1^* y_1^* + x_2^* y_2^* + x_3^* y_3^* + x_4^* y_4^* + x_5^* y_5^* + x_6^* y_6^*$$

$$= x_1^* y_1^* + x_2^* y_2^* + x_3^* y_3^* + x_3^*(-y_3^*) + x_2^*(-y_2^*) + x_1^*(-y_1^*) = 0$$

$$\sum_{i=1}^{6} (x_i^*)^2 = (x_1^*)^2 + (x_2^*)^2 + (x_3^*)^2 + (x_4^*)^2 + (x_5^*)^2 + (x_6^*)^2 = 2[(x_1^*)^2 + (x_2^*)^2 + (x_3^*)^2]$$

$$= 2 [(x_{J1} - X_{B1})^2 + (x_{J2} - X_{B2})^2 + (x_{J3} - X_{B3})^2]$$

$$= 2 [x_{J1}^2 + x_{J2}^2 + x_{J3}^2 + X_{B1}^2 + X_{B2}^2 + X_{B3}^2 - 2x_{J1}X_{B1} - 2x_{J2}X_{B2} - 2x_{J3}X_{B3}]$$

$$= 2 \{r^2[s^2(\pi/6 + \varphi2) + s^2(\pi/6 - \varphi2) + c^2(\varphi2)] + R^2[c^2(\varphi1) + s^2(\pi/6 - \varphi1)$$

$$+ s^2(\pi/6 + \varphi1)] - 2rR[s(\pi/6 + \varphi2)c(\varphi1) - s(\pi/6 - \varphi2)s(\pi/6 - \varphi1)$$

$$+ c(\varphi2)s(\pi/6 + \varphi1)]\}$$

$$= 2 \{r^2[\tfrac{1}{4}c^2(\varphi2) + \tfrac{3}{4}s^2(\varphi2) + \tfrac{\sqrt{3}}{2}s(\varphi2)c(\varphi2) + \tfrac{1}{4}c^2(\varphi2) + \tfrac{3}{4}s^2(\varphi2)$$

$$- \tfrac{\sqrt{3}}{2}s(\varphi2)c(\varphi2) + c^2(\varphi2)] + R^2[c^2(\varphi1) + \tfrac{1}{4}c^2(\varphi1) + \tfrac{3}{4}s^2(\varphi1)$$

$$- \tfrac{\sqrt{3}}{2}s(\varphi1)c(\varphi1) + \tfrac{1}{4}c^2(\varphi1) + \tfrac{3}{4}s^2(\varphi1) + \tfrac{\sqrt{3}}{2}s(\varphi1)c(\varphi1)]$$

$$- 2rR[\tfrac{1}{2}c(\varphi1)c(\varphi2) + \tfrac{\sqrt{3}}{2}c(\varphi1)s(\varphi2) - \tfrac{1}{4}c(\varphi1)c(\varphi2)$$

$$+ \tfrac{\sqrt{3}}{4}s(\varphi1)c(\varphi2) + \tfrac{\sqrt{3}}{4}c(\varphi1)s(\varphi2) - \tfrac{3}{4}s(\varphi1)s(\varphi2) + \tfrac{1}{2}c(\varphi1)c(\varphi2)$$

$$+ \tfrac{\sqrt{3}}{2}s(\varphi1)c(\varphi2)]\}$$

$$= 2\{\tfrac{3}{2}r^2 + \tfrac{3}{2}R^2 - 2rR\tfrac{3}{2}[\tfrac{1}{2}c(\varphi1 + \varphi2) + \tfrac{\sqrt{3}}{2}s(\varphi1 + \varphi2)]\}$$

$$= 3[r^2 + R^2 - 2rRs(\pi/6 + \varphi1 + \varphi2)] = 3[r^2 + R^2 - 2rRc(\pi/3 - \varphi1 - \varphi2)]$$

$$= 3r^{*2}$$

where $r^{*2} = r^2 + R^2 - 2rR\sin(\pi/6 + \varphi1 + \varphi2) = r^2 + R^2 - 2rR\cos(\pi/3 - \varphi1 - \varphi2)$

$$\sum_{i=1}^{6} (y_i^*)^2 = (y_1^*)^2 + (y_2^*)^2 + (y_3^*)^2 + (y_4^*)^2 + (y_5^*)^2 + (y_6^*)^2 = 2[(y_1^*)^2 + (y_2^*)^2 + (y_3^*)^2]$$

$$= 2\,[(y_{J1} - Y_{B1})^2 + (y_{J2} - Y_{B2})^2 + (y_{J3} - Y_{B3})^2]$$

$$= 2\,[y_{J1}^2 + y_{J2}^2 + y_{J3}^2 + Y_{B1}^2 + Y_{B2}^2 + Y_{B3}^2 - 2y_{J1}Y_{B1} - 2y_{J2}Y_{B2} - 2y_{J3}Y_{B3}]$$

$$= 2\,\{r^2[c^2(\pi/6 + \varphi 2) + c^2(\pi/6 - \varphi 2) + s^2(\varphi 2)] + R^2[s^2(\varphi 1) + c^2(\pi/6 - \varphi 1)$$

$$+ c^2(\pi/6 + \varphi 1)] - 2rR[c(\pi/6 + \varphi 2)s(\varphi 1) + c(\pi/6 - \varphi 2)c(\pi/6 - \varphi 1)$$

$$+ s(\varphi 2)c(\pi/6 + \varphi 1)]\}$$

$$= 2\,\{r^2[\tfrac{3}{4}c^2(\varphi 2) + \tfrac{1}{4}s^2(\varphi 2) - \tfrac{\sqrt{3}}{2}s(\varphi 2)c(\varphi 2) + \tfrac{3}{4}c^2(\varphi 2) + \tfrac{1}{4}s^2(\varphi 2)$$

$$+ \tfrac{\sqrt{3}}{2}s(\varphi 2)c(\varphi 2) + s^2(\varphi 2)] + R^2[s^2(\varphi 1) + \tfrac{3}{4}c^2(\varphi 1) + \tfrac{1}{4}s^2(\varphi 1)$$

$$+ \tfrac{\sqrt{3}}{2}s(\varphi 1)c(\varphi 1) + \tfrac{3}{4}c^2(\varphi 1) + \tfrac{1}{4}s^2(\varphi 1) - \tfrac{\sqrt{3}}{2}s(\varphi 1)c(\varphi 1)]$$

$$- 2rR[\tfrac{\sqrt{3}}{2}s(\varphi 1)c(\varphi 2) - \tfrac{1}{2}s(\varphi 1)s(\varphi 2) + \tfrac{3}{4}c(\varphi 1)c(\varphi 2)$$

$$+ \tfrac{\sqrt{3}}{4}s(\varphi 1)c(\varphi 2) + \tfrac{\sqrt{3}}{4}c(\varphi 1)s(\varphi 2) + \tfrac{1}{4}s(\varphi 1)s(\varphi 2) + \tfrac{\sqrt{3}}{2}c(\varphi 1)s(\varphi 2)$$

$$- \tfrac{1}{2}s(\varphi 1)s(\varphi 2)]\}$$

$$= 2\,\{\tfrac{3}{2}r^2 + \tfrac{3}{2}R^2 - 2rR\tfrac{3}{2}[\tfrac{1}{2}c(\varphi 1 + \varphi 2) + \tfrac{\sqrt{3}}{2}s(\varphi 1 + \varphi 2)]\}$$

$$= 3[r^2 + R^2 - 2rRs(\pi/6 + \varphi 1 + \varphi 2)] = 3[r^2 + R^2 - 2rRc(\pi/3 - \varphi 1 - \varphi 2)]$$

$$= 3r^{*2}$$

$$\sum_{i=1}^{6} (x_{Ji})^2 = x_{J1}^2 + x_{J2}^2 + x_{j3}^2 + x_{j4}^2 + x_{J5}^2 + x_{j6}^2 = 2[x_{j1}^2 + x_{J2}^2 + x_{J3}^2] = 3r^2$$

$$\sum_{i=1}^{6} (y_{Ji})^2 = y_{J1}^2 + y_{J2}^2 + y_{J3}^2 + y_{J4}^2 + y_{J5}^2 + y_{J6}^2 = 2[y_{J1}^2 + y_{J2}^2 + y_{J3}^2] = 3r^2$$

$$\sum_{i=1}^{6} (X_{Bi})^2 = 2[X_{B1}^2 + X_{B2}^2 + X_{B3}^2] = 3R^2$$

$$\sum_{i=1}^{6} (Y_{Bi})^2 = 2[Y_{B1}{}^2 + y_{B2}{}^2 + Y_{B3}{}^2] = 3R^2$$

$$\sum_{i=1}^{6} x_{Ji}X_{Bi} = 2(x_{J1}X_{B1} + x_{J2}X_{B2} + x_{J3}X_{B3}) = -\frac{1}{2}(3C - 3r^2 - 3R^2)$$

$$= 3rR\sin(\pi/6 + \varphi1 + \varphi2)$$

$$\sum_{i=1}^{6} y_{Ji}Y_{Bi} = 2(y_{J1}Y_{B1} + y_{J2}Y_{B2} + y_{J3}Y_{B3}) = -\frac{1}{2}(3C - 3r^2 - 3R^2)$$

$$= 3rR\sin(\pi/6 + \varphi1 + \varphi2)$$

$$\sum_{i=1}^{6} x_{Ji}Y_{Bi}^2 = 2(x_{J1}Y_{B1}^2 + x_{J2}Y_{B2}^2 + x_{J3}Y_{B3}^2) = 2rR^2[s^2(\varphi1)s(\pi/6 + \varphi2)$$

$$+c^2(\pi/6 - \varphi1)s(\pi/6 - \varphi2) - c^2(\pi/6 + \varphi1)c(\varphi2)] = 2rR^2[-\frac{3}{8}c(\varphi2)c^2(\varphi1)$$

$$+\frac{3}{8}c(\varphi2)s^2(\varphi1) - \frac{3\sqrt{3}}{8}s(\varphi2)c^2(\varphi1) + \frac{3\sqrt{3}}{8}s(\varphi2)s^2(\varphi1) + \frac{3}{4}s(\varphi1)c(\varphi1)\sqrt{3}c(\varphi2)$$

$$-\frac{3}{4}s(\varphi1)c(\varphi1)s(\varphi2)] = 2rR^2[-\frac{3}{4}c(2\varphi1)s(\pi/6 + \varphi2) + \frac{3}{4}s(2\varphi1)c(\pi/6 + \varphi2)]$$

$$= -\frac{3}{2}rR^2s(\pi/6 + \varphi2 - 2\varphi1)$$

$$\sum_{i=1}^{6} y_{Ji}^2X_{Bi} = 2(y_{J1}^2X_{B1} + y_{J2}^2X_{B2} + y_{J3}^2X_{B3}) = 2r^2R[c^2(\pi/6 + \varphi2)c(\varphi1)$$

$$-c^2(\pi/6 - \varphi2)s(\pi/6 - \varphi1) - s^2(\varphi2)s(\pi/6 + \varphi1)] = \frac{3}{2}r^2Rs(\pi/6 + \varphi1 - 2\varphi2)$$

(permutation of the subscripts)

$$\sum_{i=1}^{6} x_{Ji}y_{Ji}Y_{Bi} = 2(x_{J1}y_{J1}Y_{B1} + x_{J2}y_{J2}Y_{B2} + x_{J3}y_{J3}Y_{B3})$$

$$= 2r^2R[s(\pi/6 + \varphi2)c(\pi/6 + \varphi2)s(\varphi1) + s(\pi/6 - \varphi2)c(\pi/6 - \varphi2)c(\pi/6 - \varphi1)$$

$$-c(\varphi2)s(\varphi2)c(\pi/6 + \varphi1)] = 2r^2R[\frac{3\sqrt{3}}{8}s(\varphi1)c(2\varphi2) - \frac{3\sqrt{3}}{8}c(\varphi1)s(2\varphi2)$$

$$+\frac{3}{8}c(\varphi1)c(2\varphi2) + \frac{3}{8}s(\varphi1)s(2\varphi2)] = \frac{3}{2}r^2R[c(2\varphi2)s(\pi/6 + \varphi1)$$

$$-s(2\varphi2)c(\pi/6+\varphi1)] = \tfrac{3}{2}r^2Rs(\pi/6+\varphi1-2\varphi2)$$

$$\sum_{i=1}^{6} y_{Ji}X_{Bi}Y_{Bi} = 2(y_{J1}X_{B1}Y_{B1}+y_{J2}X_{B2}Y_{B2}+y_{J3}X_{B3}Y_{B3})$$

$$=2rR^2[c(\pi/6+\varphi2)c(\varphi1)s(\varphi1)-c(\pi/6-\varphi2)s(\pi/6-\varphi1)c(\pi/6-\varphi1)$$
$$-s(\varphi2)s(\pi/6+\varphi1)c(\pi/6+\varphi1)] = -\tfrac{3}{2}rR^2s(\pi/6+\varphi2-2\varphi1)$$

(permutation of the subscripts)

$$\sum_{i=1}^{6} y_{Ji}^2X_{Bi}^2 = 2(y_{J1}^2X_{B1}^2+y_{J2}^2X_{B2}^2+y_{J3}^2X_{B3}^2) = 2r^2R^2[c^2(\varphi1)c^2(\pi/6+\varphi2)$$

$$+c^2(\pi/6-\varphi2)s^2(\pi/6-\varphi1)+s^2(\varphi2)s^2(\pi/6+\varphi1)] = 2r^2R^2[\tfrac{15}{16}c^2(\varphi1)c^2(\varphi2)$$

$$+\tfrac{9}{16}c^2(\varphi1)s^2(\varphi2)+\tfrac{15}{16}s^2(\varphi1)s^2(\varphi2)+\tfrac{9}{16}s^2(\varphi1)c^2(\varphi2)+\tfrac{3\sqrt{3}}{8}c^2(\varphi1)s(\varphi2)c(\varphi2)$$

$$+\tfrac{3\sqrt{3}}{8}s^2(\varphi1)s(\varphi2)c(\varphi2)+\tfrac{3\sqrt{3}}{8}s^2(\varphi2)s(\varphi1)c(\varphi1)-\tfrac{3\sqrt{3}}{8}c^2(\varphi2)s(\varphi1)c(\varphi1)$$

$$-\tfrac{3}{4}s(\varphi1)s(\varphi2)c(\varphi1)c(\varphi2) = 2r^2R^2\{\tfrac{15}{16}[c(\varphi1)c(\varphi2)-s(\varphi1)s(\varphi2)]^2$$

$$+\tfrac{9}{16}[c(\varphi1)s(\varphi2)+s(\varphi1)c(\varphi2)]^2-\tfrac{3\sqrt{3}}{16}[s(2\varphi1)c(2\varphi2)+c(2\varphi1)s(2\varphi2)]\}$$

$$=\tfrac{3}{8}r^2R^2[5c^2(\varphi1+\varphi2)+3s^2(\varphi1+\varphi2)-\sqrt{3}s(2\varphi1+2\varphi2)]$$

$$=\tfrac{3}{8}r^2R^2[3+2c^2(\varphi1+\varphi2)-\sqrt{3}s(2\varphi1+2\varphi2)]$$

$$\sum_{i=1}^{6} x_{Ji}^2Y_{Bi}^2 = 2(x_{J1}^2Y_{B1}^2+x_{J2}^2Y_{B2}^2+x_{J3}^2Y_{B3}^2) = 2r^2R^2[s^2(\varphi1)s^2(\pi/6+\varphi2)$$

$$+c^2(\pi/6-\varphi1)s^2(\pi/6-\varphi2)+c^2(\varphi2)c^2(\pi/6+\varphi1)]$$

$$=\tfrac{3}{8}r^2R^2[3+2c^2(\varphi1+\varphi2)-\sqrt{3}s(2\varphi1+2\varphi2)]$$

(permutation of the subscripts)

$$\sum_{i=1}^{6} x_{Ji}y_{Ji}X_{Bi}Y_{Bi}=2(x_{J1}y_{J1}X_{B1}Y_{B1}+x_{J2}y_{J2}X_{B2}Y_{B2}+x_{J3}y_{J3}X_{B3}Y_{B3})$$

$$=2r^2R^2[\tfrac{1}{4}s(\pi/3+2\varphi2)s(2\varphi1)-\tfrac{1}{4}s(\pi/3-2\varphi2)s(\pi/3-2\varphi1)+\tfrac{1}{4}s(2\varphi2)s(\pi/3+2\varphi1)]$$

$$= \frac{1}{2} r^2 R^2 [\frac{3}{4} s(2\varphi 1) s(2\varphi 2) - \frac{3}{4} c(2\varphi 1) cs(2\varphi 2) + \frac{3\sqrt{3}}{4} s(2\varphi 1) c(2\varphi 2)$$

$$+ \frac{3\sqrt{3}}{4} c(2\varphi 1) s(2\varphi 2)] = \frac{3}{4} r^2 R^2 [\frac{1}{2} c(2\varphi 1 + 2\varphi 2) - \frac{\sqrt{3}}{2} s(2\varphi 1 + 2\varphi 2)]$$

$$= -\frac{3}{4} r^2 R^2 s(\pi/6 - 2\varphi 1 - 2\varphi 2)$$

Appendix 2.2

Eqn. (2.17) gives $\mathbf{l}_i = \begin{Bmatrix} l_{iX} \\ l_{iY} \\ l_{iZ} \end{Bmatrix} = \begin{Bmatrix} D_{11}x_{Ji}+D_{12}y_{Ji}+x-x_{Bi} \\ D_{21}x_{Ji}+D_{22}y_{Ji}+y-y_{Bi} \\ D_{31}x_{Ji}+D_{32}y_{Ji}+z \end{Bmatrix}$

and Eqn. (2.16b) shows $\mathbf{l}_i$ described in platform coordinates, i.e., xyz frame,

$$\mathbf{l}_i = \begin{Bmatrix} l_{ix} \\ l_{iy} \\ l_{iz} \end{Bmatrix} = \begin{Bmatrix} \mathbf{l}_i \cdot \mathbf{D}_1 \\ \mathbf{l}_i \cdot \mathbf{D}_2 \\ \mathbf{l}_i \cdot \mathbf{D}_3 \end{Bmatrix}$$

where the direction vectors $\mathbf{D}_1$, $\mathbf{D}_2$, and $\mathbf{D}_3$ are given by Eqn. (2.15)

$$\mathbf{D}_1 = \begin{Bmatrix} D_{11} \\ D_{21} \\ D_{31} \end{Bmatrix} = \begin{Bmatrix} \cos\beta\cos\gamma \\ \cos\beta\sin\gamma \\ -\sin\beta \end{Bmatrix}$$

$$\mathbf{D}_2 = \begin{Bmatrix} D_{12} \\ D_{22} \\ D_{32} \end{Bmatrix} = \begin{Bmatrix} \sin\alpha\sin\beta\cos\gamma-\cos\alpha\sin\gamma \\ \sin\alpha\sin\beta\sin\gamma+\cos\alpha\cos\gamma \\ \sin\alpha\cos\beta \end{Bmatrix}$$

$$\mathbf{D}_3 = \begin{Bmatrix} D_{13} \\ D_{23} \\ D_{33} \end{Bmatrix} = \begin{Bmatrix} \cos\alpha\sin\beta\cos\gamma+\sin\alpha\sin\gamma \\ \cos\alpha\sin\beta\sin\gamma-\sin\alpha\cos\gamma \\ \cos\alpha\cos\beta \end{Bmatrix}$$

the leg length is given by Eqn. (2.18)

$$l_i = \sqrt{l_{iX}^2 + l_{iY}^2 + l_{iZ}^2}$$

and the Jacobian matrix will be

$$[J] = \left[\frac{\partial l}{\partial x}\right] = [J_{ij}] = \left[\frac{\partial l_i}{\partial x_j}\right] = \begin{bmatrix} \dfrac{\partial l_1}{\partial x} & \dfrac{\partial l_1}{\partial y} & \cdots & \dfrac{\partial l_1}{\partial \gamma} \\[2mm] \dfrac{\partial l_2}{\partial x} & \dfrac{\partial l_2}{\partial y} & \cdots & \dfrac{\partial l_2}{\partial \gamma} \\[2mm] \cdots \\[1mm] \dfrac{\partial l_6}{\partial x} & \dfrac{\partial l_6}{\partial y} & \cdots & \dfrac{\partial l_6}{\partial \gamma} \end{bmatrix}$$

where

$$\frac{\partial l_i}{\partial x} = \frac{\partial(\sqrt{l_{iX}^2 + l_{iY}^2 + l_{iZ}^2}\,)}{\partial x} = \frac{2 l_{iX}\dfrac{\partial l_{iX}}{\partial x}}{2\sqrt{l_{iX}^2 + l_{iY}^2 + l_{iZ}^2}} = \frac{l_{iX}}{l_i} = \frac{D_{11}x_{Ji} + D_{12}y_{Ji} + x - X_{Bi}}{l_i}$$

$$\frac{\partial l_i}{\partial y} = \frac{\partial(\sqrt{l_{iX}^2 + l_{iY}^2 + l_{iZ}^2}\,)}{\partial y} = \frac{2 l_{iY}\dfrac{\partial l_{iY}}{\partial y}}{2\sqrt{l_{iX}^2 + l_{iY}^2 + l_{iZ}^2}} = \frac{l_{iY}}{l_i} = \frac{D_{21}x_{Ji} + D_{22}y_{Ji} + y - Y_{Bi}}{l_i}$$

$$\frac{\partial l_i}{\partial z} = \frac{\partial(\sqrt{l_{iX}^2 + l_{iY}^2 + l_{iZ}^2}\,)}{\partial z} = \frac{2 l_{iZ}\dfrac{\partial l_{iZ}}{\partial z}}{2\sqrt{l_{iX}^2 + l_{iY}^2 + l_{iZ}^2}} = \frac{l_{iZ}}{l_i} = \frac{D_{31}x_{Ji} + D_{32}y_{Ji} + z}{l_i}$$

since

$$\frac{\partial D_1}{\partial \alpha} = \begin{Bmatrix} \dfrac{\partial D_{11}}{\partial \alpha} \\[2mm] \dfrac{\partial D_{21}}{\partial \alpha} \\[2mm] \dfrac{\partial D_{31}}{\partial \alpha} \end{Bmatrix} = 0$$

$$\frac{\partial D_2}{\partial \alpha} = \begin{Bmatrix} \dfrac{\partial D_{12}}{\partial \alpha} \\[2mm] \dfrac{\partial D_{22}}{\partial \alpha} \\[2mm] \dfrac{\partial D_{32}}{\partial \alpha} \end{Bmatrix} = \begin{Bmatrix} \cos\alpha\sin\beta\cos\gamma + \sin\alpha\sin\gamma \\[2mm] \cos\alpha\sin\beta\sin\gamma - \sin\alpha\cos\gamma \\[2mm] \cos\alpha\cos\beta \end{Bmatrix} = D_3$$

$$\frac{\partial \mathbf{D}_3}{\partial \alpha} = \left\{ \begin{array}{c} \frac{\partial D_{13}}{\partial \alpha} \\ \frac{\partial D_{23}}{\partial \alpha} \\ \frac{\partial D_{33}}{\partial \alpha} \end{array} \right\} = \left\{ \begin{array}{c} -\sin\alpha\sin\beta\cos\gamma + \cos\alpha\sin\gamma \\ -\sin\alpha\sin\beta\sin\gamma - \cos\alpha\cos\gamma \\ -\sin\alpha\cos\beta \end{array} \right\} = -\mathbf{D}_2$$

$$\frac{\partial \mathbf{D}_1}{\partial \beta} = \left\{ \begin{array}{c} \frac{\partial D_{11}}{\partial \beta} \\ \frac{\partial D_{21}}{\partial \beta} \\ \frac{\partial D_{31}}{\partial \beta} \end{array} \right\} = \left\{ \begin{array}{c} -\sin\beta\cos\gamma \\ -\sin\beta\sin\gamma \\ -\cos\beta \end{array} \right\} = -(\sin\alpha\mathbf{D}_2 + \cos\alpha\mathbf{D}_3)$$

$$\frac{\partial \mathbf{D}_2}{\partial \beta} = \left\{ \begin{array}{c} \frac{\partial D_{12}}{\partial \beta} \\ \frac{\partial D_{22}}{\partial \beta} \\ \frac{\partial D_{32}}{\partial \beta} \end{array} \right\} = \left\{ \begin{array}{c} \sin\alpha\cos\beta\cos\gamma \\ \sin\alpha\cos\beta\sin\gamma \\ -\sin\alpha\sin\beta \end{array} \right\} = \sin\alpha\mathbf{D}_1$$

$$\frac{\partial \mathbf{D}_3}{\partial \beta} = \left\{ \begin{array}{c} \frac{\partial D_{13}}{\partial \beta} \\ \frac{\partial D_{23}}{\partial \beta} \\ \frac{\partial D_{33}}{\partial \beta} \end{array} \right\} = \left\{ \begin{array}{c} \cos\alpha\cos\beta\cos\gamma \\ \cos\alpha\cos\beta\sin\gamma \\ -\cos\alpha\sin\beta \end{array} \right\} = \cos\alpha\mathbf{D}_1$$

$$\frac{\partial \mathbf{D}_1}{\partial \gamma} = \left\{ \begin{array}{c} \frac{\partial D_{11}}{\partial \gamma} \\ \frac{\partial D_{21}}{\partial \gamma} \\ \frac{\partial D_{31}}{\partial \gamma} \end{array} \right\} = \left\{ \begin{array}{c} -\cos\beta\sin\gamma \\ \cos\beta\cos\gamma \\ 0 \end{array} \right\} = \cos\beta \left\{ \begin{array}{c} -\sin\gamma \\ \cos\gamma \\ 0 \end{array} \right\} = \cos\beta(\cos\alpha\mathbf{D}_2 - \sin\alpha\mathbf{D}_3)$$

$$\frac{\partial \mathbf{D}_2}{\partial \gamma} = \left\{ \begin{array}{c} \frac{\partial D_{12}}{\partial \gamma} \\ \frac{\partial D_{22}}{\partial \gamma} \\ \frac{\partial D_{32}}{\partial \gamma} \end{array} \right\} = \left\{ \begin{array}{c} -\sin\alpha\sin\beta\sin\gamma - \cos\alpha\cos\gamma \\ \sin\alpha\sin\beta\cos\gamma - \cos\alpha\sin\gamma \\ 0 \end{array} \right\} = -\cos\alpha\cos\beta\mathbf{D}_1 - \sin\beta\mathbf{D}_3$$

$$\frac{\partial \mathbf{D}_3}{\partial \gamma} = \begin{vmatrix} \dfrac{\partial D_{13}}{\partial \gamma} \\[6pt] \dfrac{\partial D_{23}}{\partial \gamma} \\[6pt] \dfrac{\partial D_{33}}{\partial \gamma} \end{vmatrix} = \begin{pmatrix} -\cos\alpha\sin\beta\sin\gamma+\sin\alpha\cos\gamma \\[4pt] \cos\alpha\sin\beta\cos\gamma+\sin\alpha\sin\gamma \\[4pt] 0 \end{pmatrix} = \sin\alpha\cos\beta\mathbf{D}_1+\sin\beta\mathbf{D}_2$$

so,

$$\frac{\partial l_i}{\partial \alpha} = \frac{\partial(\sqrt{l_{iX}^2+l_{iY}^2+l_{iZ}^2})}{\partial \alpha} = \frac{2l_{iX}\dfrac{\partial l_{iX}}{\partial \alpha}+2l_{iY}\dfrac{\partial l_{iY}}{\partial \alpha}+2l_{iZ}\dfrac{\partial l_{iZ}}{\partial \alpha}}{2\sqrt{l_{iX}^2+l_{iY}^2+l_{iZ}^2}}$$

$$= \frac{l_{iX}(\dfrac{\partial D_{11}}{\partial \alpha}x_{Ji}+\dfrac{\partial D_{12}}{\partial \alpha}y_{Ji})+l_{iY}(\dfrac{\partial D_{21}}{\partial \alpha}x_{Ji}+\dfrac{\partial D_{22}}{\partial \alpha}y_{Ji})+l_{iZ}(\dfrac{\partial D_{31}}{\partial \alpha}x_{Ji}+\dfrac{\partial D_{32}}{\partial \alpha}y_{Ji})}{l_i}$$

$$= \frac{x_{Ji}(\mathbf{l}_i\cdot\dfrac{\partial \mathbf{D}_1}{\partial \alpha})+y_{Ji}(\mathbf{l}_i\cdot\dfrac{\partial \mathbf{D}_2}{\partial \alpha})}{l_i} = \frac{y_{Ji}(\mathbf{l}_i\cdot\mathbf{D}_3)}{l_i} = y_{Ji}\frac{l_{iz}}{l_i}$$

$$\frac{\partial l_i}{\partial \beta} = \frac{\partial(\sqrt{l_{iX}^2+l_{iY}^2+l_{iZ}^2})}{\partial \beta} = \frac{2l_{iX}\dfrac{\partial l_{iX}}{\partial \beta}+2l_{iY}\dfrac{\partial l_{iY}}{\partial \beta}+2l_{iZ}\dfrac{\partial l_{iZ}}{\partial \beta}}{2\sqrt{l_{iX}^2+l_{iY}^2+l_{iZ}^2}}$$

$$= \frac{l_{iX}(\dfrac{\partial D_{11}}{\partial \beta}x_{Ji}+\dfrac{\partial D_{12}}{\partial \beta}y_{Ji})+l_{iY}(\dfrac{\partial D_{21}}{\partial \beta}x_{Ji}+\dfrac{\partial D_{22}}{\partial \beta}y_{Ji})+l_{iZ}(\dfrac{\partial D_{31}}{\partial \beta}x_{Ji}+\dfrac{\partial D_{32}}{\partial \beta}y_{Ji})}{l_i}$$

$$= \frac{x_{Ji}(\mathbf{l}_i\cdot\dfrac{\partial \mathbf{D}_1}{\partial \beta})+y_{Ji}(\mathbf{l}_i\cdot\dfrac{\partial \mathbf{D}_2}{\partial \beta})}{l_i} = \frac{-x_{Ji}[\sin\alpha(\mathbf{l}_i\cdot\mathbf{D}_2)+\cos\alpha(\mathbf{l}_i\cdot\dot{\mathbf{D}}_3)]+y_{Ji}\sin\alpha(\mathbf{l}_i\cdot\mathbf{D}_1)}{l_i}$$

$$= \frac{\mathbf{l}_i\cdot(y_{Ji}\sin\alpha\mathbf{D}_1-x_{Ji}\sin\alpha\mathbf{D}_2-x_{Ji}\cos\alpha\mathbf{D}_3)}{l_i} = y_{Ji}\sin\alpha\frac{l_{ix}}{l_i}-x_{Ji}\sin\alpha\frac{l_{iy}}{l_i}-x_{Ji}\cos\alpha\frac{l_{iz}}{l_i}$$

$$\frac{\partial l_i}{\partial \gamma} = \frac{\partial(\sqrt{l_{iX}^2+l_{iY}^2+l_{iZ}^2})}{\partial \gamma} = \frac{2l_{iX}\dfrac{\partial l_{iX}}{\partial \gamma}+2l_{iY}\dfrac{\partial l_{iY}}{\partial \gamma}+2l_{iZ}\dfrac{\partial l_{iZ}}{\partial \gamma}}{2\sqrt{l_{iX}^2+l_{iY}^2+l_{iZ}^2}}$$

$$= \frac{l_{iX}\left(\frac{\partial D_{11}}{\partial \gamma}x_{Ji}+\frac{\partial D_{12}}{\partial \gamma}y_{Ji}\right)+l_{iY}\left(\frac{\partial D_{21}}{\partial \gamma}x_{Ji}+\frac{\partial D_{22}}{\partial \gamma}y_{Ji}\right)+l_{iZ}\left(\frac{\partial D_{31}}{\partial \gamma}x_{Ji}+\frac{\partial D_{32}}{\partial \gamma}y_{Ji}\right)}{l_i}$$

$$= \frac{x_{Ji}\left(\mathbf{l_i}\cdot\frac{\partial \mathbf{D}_1}{\partial \gamma}\right)+y_{Ji}\left(\mathbf{l_i}\cdot\frac{\partial \mathbf{D}_2}{\partial \gamma}\right)}{l_i}$$

$$= \frac{x_{Ji}\cos\beta[\cos\alpha(\mathbf{l_i}\cdot\mathbf{D}_2)-\sin\alpha(\mathbf{l_i}\cdot\mathbf{D}_3)-y_{Ji}[\cos\alpha\cos\beta(\mathbf{l_i}\cdot\mathbf{D}_1)+\sin\beta(\mathbf{l_i}\cdot\mathbf{D}_3)]}{l_i}$$

$$= x_{Ji}\cos\beta\left(\cos\alpha\frac{l_{iy}}{l_i}-\sin\alpha\frac{l_{iz}}{l_i}\right)-y_{Ji}\left(\cos\alpha\cos\beta\frac{l_{ix}}{l_i}+\sin\beta\frac{l_{iz}}{l_i}\right)$$

Appendix 2.3

Eqn. (2.29) gives $[S] = [J]^T [K] [J]$, so, for platform is at its rest configuration, where $x = \{0, 0, z_0, 0, 0, 0\}$ and due to symmetry of the configuration, each leg length will be same at this time, $l_i = l_0$, ($i = 1, 2,$ $\cdots$, 6), if we assume that the individual stiffness of each leg is same, i.e., $k_i = k$, ($i = 1, 2, \cdots$, 6), the stiffness matrix $[S]$ is

$$[S] = [J]^T [K] [J] = k[J]^T[J] = [S_{ij}] = k\left[\frac{\partial l_i}{\partial x_i}\right]\left[\frac{\partial l_i}{\partial x_j}\right] = k\left[\sum_{m=1}^{6} \frac{\partial l_m \partial l_m}{\partial x_i \partial x_j}\right]$$

since $x=0$, $y=0$, $z=z_0$, $\alpha=0$, $\beta=0$, $\gamma=0$, the direction vectors are

$$D_1 = \begin{Bmatrix} 1 \\ 0 \\ 0 \end{Bmatrix} \qquad D_2 = \begin{Bmatrix} 0 \\ 1 \\ 0 \end{Bmatrix} \qquad D_3 = \begin{Bmatrix} 0 \\ 0 \\ 1 \end{Bmatrix}$$

and the components of leg length are

$$l_{ix} = l_{iX} = D_{11}x_{Ji} + D_{12}y_{Ji} + x - X_{Bi} = x_i^*$$

$$l_{iy} = l_{iY} = D_{21}x_{Ji} + D_{22}y_{Ji} + y - Y_{Bi} = y_i^*$$

$$l_{iz} = l_{iZ} = D_{31}x_{Ji} + D_{32}y_{Ji} + z_0 = z_0$$

so,

$$\frac{\partial l_i}{\partial x} = \frac{l_{iX}}{l_i} = \frac{x_i^*}{l_0}$$

$$\frac{\partial l_i}{\partial y} = \frac{l_{iY}}{l_i} = \frac{y_i^*}{l_0}$$

$$\frac{\partial l_i}{\partial z} = \frac{l_{iZ}}{l_i} = \frac{z_0}{l_0}$$

$$\frac{\partial l_i}{\partial \alpha} = y_{Ji}\frac{l_{iZ}}{l_i} = y_{Ji}\frac{z_0}{l_0}$$

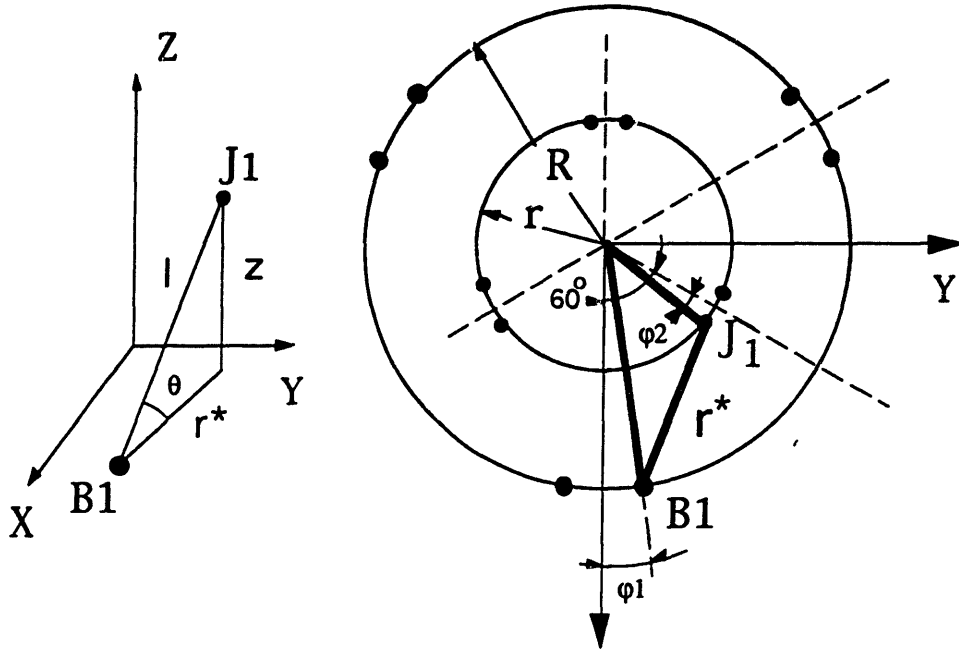$$\frac{\partial l_i}{\partial \beta} = -x_{Ji}\frac{l_{iZ}}{l_i} = -x_{Ji}\frac{z_0}{l_0}$$

$$\frac{\partial l_i}{\partial \gamma} = x_{Ji}\frac{l_{iY}}{l_i} - y_{Ji}\frac{l_{iX}}{l_i} = \frac{X_{Bi}y_{Ji} - x_{Ji}Y_{Bi}}{l_0}$$

and

$$S_{11} = k\sum_{i=1}^{6}(\frac{\partial l_i}{\partial x})^2 = k\sum_{i=1}^{6}(\frac{x_i^*}{l_0})^2 = \frac{k}{l_0^2}(\sum_{i=1}^{6}(x_i^*)^2) = \frac{3kr^{*2}}{l_0^2}$$

where

$$r^{*2} = r^2 + R^2 - 2rR\sin(\pi/6 + \varphi1 + \varphi2) = r^2 + R^2 - 2rR\cos(\pi/3 - \varphi1 - \varphi2)$$

From the above figure, we have

$$\sin\theta = \frac{z_0}{l_0} \quad \text{and} \quad \cos\theta = \frac{r^*}{l_0}$$

so,

$$S_{11} = \frac{3kr^{*2}}{l_0^2} = 3k\cos^2\theta$$

$$S_{22} = k\sum_{i=1}^{6}(\frac{\partial l_i}{\partial y})^2 = k\sum_{i=1}^{6}(\frac{y_i^*}{l_0})^2 = \frac{k}{l_0^2}(\sum_{i=1}^{6}(y_i^*)^2) = \frac{3kr^{*2}}{l_0^2} = 3k\cos^2\theta$$

$$S_{33} = k\sum_{i=1}^{6}(\frac{\partial l_i}{\partial z})^2 = k\sum_{i=1}^{6}(\frac{z_0}{l_0})^2 = 6k\frac{z_0^2}{l_0^2} = 6k\sin^2\theta$$

$$S_{44} = k\sum_{i=1}^{6}(\frac{\partial l_i}{\partial \alpha})^2 = k\sum_{i=1}^{6}(y_{Ji}\frac{z_0}{l_0})^2 = k\frac{z_0^2}{l_0^2}\sum_{i=1}^{6}y_{Ji}^2 = 3kr^2\frac{z_0^2}{l_0^2} = 3kr^2\sin^2\theta$$

$$S_{55} = k\sum_{i=1}^{6}(\frac{\partial l_i}{\partial \beta})^2 = k\sum_{i=1}^{6}(-x_{Ji}\frac{z_0}{l_0})^2 = k\frac{z_0^2}{l_0^2}\sum_{i=1}^{6}x_{Ji}^2 = 3kr^2\frac{z_0^2}{l_0^2} = 3kr^2\sin^2\theta$$

$$S_{66} = k\sum_{i=1}^{6}(\frac{\partial l_i}{\partial \gamma})^2 = k\sum_{i=1}^{6}(\frac{y_{Ji}X_{Bi}-x_{Ji}Y_{Bi}}{l_i})^2$$

$$= \frac{k}{l_0^2}(\sum_{i=1}^{6}y_{Ji}^2 X_{Bi}^2 + \sum_{i=1}^{6}x_{Ji}^2 Y_{Bi}^2 - 2\sum_{i=1}^{6}x_{Ji}y_{Ji}X_{Bi}Y_{BJi})$$

$$= \frac{k}{l_0^2}\{2\frac{3}{8}r^2R^2[3+2c^2(\varphi1+\varphi2)-\sqrt{3}s(2\varphi1+2\varphi2)]-2[-\frac{3}{4}r^2R^2s(\pi/6-2\varphi1-2\varphi2)]\}$$

$$= \frac{kr^2R^2}{l_0^2}[\frac{9}{4}+\frac{3}{2}c^2(\varphi1+\varphi2)-\frac{3\sqrt{3}}{2}s(2\varphi1+2\varphi2)+\frac{3}{4}c(2\varphi1+2\varphi2)]$$

$$= \frac{kr^2R^2}{l_0^2}\{\frac{9}{4}+\frac{3}{4}[2c^2(\varphi1+\varphi2)-c(2\varphi1+2\varphi2)]+3s(\pi/6-2\varphi1-2\varphi2)\}$$

$$= \frac{3kr^2R^2}{l_0^2}[1+s(\pi/6-2\varphi1-2\varphi2)]$$

$$S_{12} = S_{21} = k \sum_{i=1}^{6} \left(\frac{\partial l_i \partial l_i}{\partial x \partial y} \right) = \frac{k}{l_0^2} \left(\sum_{i=1}^{6} x_{Ji}^* y_{Ji}^* \right) = 0$$

$$S_{13} = S_{31} = k \sum_{i=1}^{6} \left(\frac{\partial l_i \partial l_i}{\partial x \partial z} \right) = k \frac{z_0}{l_0^2} \left(\sum_{i=1}^{6} x_{Ji}^* \right) = 0$$

$$S_{14} = S_{41} = k \sum_{i=1}^{6} \left(\frac{\partial l_i \partial l_i}{\partial x \partial \alpha} \right) = k \frac{z_0}{l_0^2} \left(\sum_{i=1}^{6} x_{Ji}^* y_{Ji} \right) = 0$$

$$S_{15} = S_{51} = k \sum_{i=1}^{6} \left(\frac{\partial l_i \partial l_i}{\partial x \partial \beta} \right) = \frac{-kz_0}{l_0^2} \left(\sum_{i=1}^{6} x_{Ji}^* x_{Ji} \right) = \frac{-kz_0}{l_0^2} [3r^2 - 3rRs(\pi/6 + \varphi 1 + \varphi 2)]$$

$$S_{16} = S_{61} = k \sum_{i=1}^{6} \left(\frac{\partial l_i \partial l_i}{\partial x \partial \gamma} \right) = \frac{k}{l_0^2} \left(\sum_{i=1}^{6} [x_{Ji}^*(y_{Ji} X_{Bi} - x_{Ji} Y_{Bi})] \right)$$

$$= \frac{k}{l_0^2} \left[\sum_{i=1}^{6} (x_{Ji} y_{Ji} X_{Bi}) - \sum_{i=1}^{6} (x_{Ji} X_{Bi} Y_{Bi}) \right] = 0$$

$$S_{23} = S_{32} = k \sum_{i=1}^{6} \left(\frac{\partial l_i \partial l_i}{\partial y \partial z} \right) = \frac{kz_0}{l_0^2} \left(\sum_{i=1}^{6} y_{Ji}^* \right) = 0$$

$$S_{24} = S_{42} = k \sum_{i=1}^{6} \left(\frac{\partial l_i \partial l_i}{\partial y \partial \alpha} \right) = \frac{kz_0}{l_0^2} \left(\sum_{i=1}^{6} y_{Ji}^* y_{Ji} \right) = \frac{3kz_0}{l_0^2} [r^2 - 3rRs(\pi/6 + \varphi 1 + \varphi 2)]$$

$$S_{25} = S_{52} = k \sum_{i=1}^{6} \left(\frac{\partial l_i \partial l_i}{\partial y \partial \beta} \right) = \frac{-kz_0}{l_0^2} \left(\sum_{i=1}^{6} y_{Ji}^* x_{Ji} \right) = 0$$

$$S_{26} = S_{62} = k \sum_{i=1}^{6} \left(\frac{\partial l_i \partial l_i}{\partial y \partial \gamma} \right) = \frac{k}{l_0^2} \left\{ \sum_{i=1}^{6} [y_{Ji}^*(y_{Ji} X_{Bi} - (x_{Ji} Y_{Bi}))] \right\}$$

$$= \frac{k}{l_0^2} \left[\sum_{i=1}^{6} (y_{Ji}^2 X_{Bi}) - \sum_{i=1}^{6} (x_{Ji} y_{Ji} Y_{Bi}) + \sum_{i=1}^{6} (x_{Ji} Y_{Bi}^2) - \sum_{i=1}^{6} (y_{Ji} X_{Bi} Y_{Bi}) \right] = 0$$

$$S_{34} = S_{43} = k\sum_{i=1}^{6}\left(\frac{\partial l_i}{\partial z}\frac{\partial l_i}{\partial \alpha}\right) = k\frac{z_0^2}{l_0^2}\left(\sum_{i=1}^{6} y_{Ji}\right) = 0$$

$$S_{35} = S_{53} = k\sum_{i=1}^{6}\left(\frac{\partial l_i}{\partial z}\frac{\partial l_i}{\partial \beta}\right) = \frac{-kz_0^2}{l_0^2}\left(\sum_{i=1}^{6} x_{Ji}\right) = 0$$

$$S_{36} = S_{63} = k\sum_{i=1}^{6}\left(\frac{\partial l_i}{\partial z}\frac{\partial l_i}{\partial \gamma}\right) = \frac{kz_0}{l_0^2}\left[\sum_{i=1}^{6} (y_{Ji}X_{Bi}) - \sum_{i=1}^{6} (x_{Ji}Y_{Bi})\right] = 0$$

$$S_{45} = S_{54} = k\sum_{i=1}^{6}\left(\frac{\partial l_i}{\partial \alpha}\frac{\partial l_i}{\partial \beta}\right) = \frac{-kz_0^2}{l_0^2}\left[\sum_{i=1}^{6} (x_{Ji}y_{Ji})\right] = 0$$

$$S_{46} = S_{64} = k\sum_{i=1}^{6}\left(\frac{\partial l_i}{\partial \alpha}\frac{\partial l_i}{\partial \gamma}\right) = \frac{kz_0}{l_0^2}\left[\sum_{i=1}^{6} (y_{Ji}^2 X_{Bi}) - \sum_{i=1}^{6} (x_{Ji}y_{Ji}Y_{Bi})\right] = 0$$

$$S_{56} = S_{65} = k\sum_{i=1}^{6}\left(\frac{\partial l_i}{\partial \beta}\frac{\partial l_i}{\partial \gamma}\right) = \frac{-kz_0}{l_0^2}\left[\sum_{i=1}^{6} (x_{Ji}y_{Ji}X_{Bi}) - \sum_{i=1}^{6} (x_{Ji}^2 Y_{Bi})\right] = 0$$

We know that if displacement only in x direction, i.e., $\Delta x = \{\Delta x\ 0\ 0\ 0\ 0\ 0\}^t$, the corresponding force will be

$$F_x = S_{11}\Delta x$$

so, the stiffness in x direction is

$$S_x = F_x/\Delta x = S_{11} = 3kcos^2\theta$$

and if displacement only in y direction, i.e., $\Delta x = \{0\ \Delta y\ 0\ 0\ 0\ 0\}^t$, the corresponding force will be

$$F_y = S_{22}\Delta y$$

so, the stiffness in y direction is

$$S_y = F_y/\Delta y = S_{22} = 3k\cos^2\theta$$

if in oxy plane, there is a displacement $\Delta\rho$ in the direction at the angle ψ with x axis, i.e., $\Delta x = (\Delta\rho\cos\psi \quad \Delta\rho\sin\psi \; 0 \; 0 \; 0 \; 0)^t$, and the corresponding force is

$$F_x = S_{11}\Delta\rho\cos\psi \quad \text{and} \quad F_y = S_{22}\Delta\rho\sin\psi$$

the force in ψ direction is then

$$F_\psi = \sqrt{F_x^2 + F_y^2} = \sqrt{(S_{11}\Delta\rho\cos\psi)^2 + (S_{22}\Delta\rho\sin\psi)^2} = 3k\cos^2\theta\Delta\rho$$

so, the stiffness in ψ direction is

$$S_\psi = F_\psi/\Delta\rho = 3k\cos^2\theta = S_x = S_y$$

the stiffness in horizontal direction at platform's rest position is the same, and is independent of direction ψ.

REFERENCES

[1] Asada, H. and Slotine, J.E., 1986, *Robot Analysis and Control* John Wiley and Sons

[2] Do, W.Q., 1985, *Dynamic Analysis of Stewart Platform,* M.S. Thesis, University of California, Los Angeles, CA

[3] Fresco, M., 1987, *The Design and Implementation of a Computer Controlled Platform with Variable Admittance,* M.S. Thesis, MIT, Cambridge, MA

[4] Ismail, A.N., 1988, *The Design and Construction of a Six Degree of Freedom Parallel Link Platform Type Manipulator,* M.S. Thesis, MIT, Cambridge, MA

[5] Stelman, N.M., 1988, *Design and Control of a Six-Degree-of-Freedom Platform with Variable Admittance,* M.S. Thesis, MIT, Cambridge, MA,

[6] West, H., Hootsmans, N., Dubowsky, S., Stelman, N., 1989, "Experimental Simulation of Manipulator Base Compliance" *Proceedings of the First International Symposium on Experimental Robotics,* Montreal, June 19-21

[7] Dubowsky, S., Tanner, A.B., 1987, "A Study of Dynamics and Control

of Mobile Manipulators Subjected to Vehicle Disturbances," *Proceedings,*
Fourth International Symposium of Robotics Research, Santa Cruz, CA

[8] Dubowsky, S., Vafa, Z., 1987, "A Virtual Manipulator Model for Space
Robotic Systems," *Proceedings of NASA Workshop on Space Telerobotics,*
Jet Propulsion Laboratory, California Institute of Technology, Pasadena,
CA

[9] Dubowsky, S., Paul, I., West, H., 1988, "An Analytical and
Experimental Program to Develop Control Algorithms for Mobile
Manipulators ," *Proc.,* RoManSy, Udine, Italy, July

[10] Powell, I. L., 1981, "The Parallel Topology Manipulator, Kinematic
Analysis and Simulation," MTR. 81/30, Chelmsford, Great Britain:
Marconi Research Laboratories, GEC Marconi Electronics Limited.

[11] Fichter, E.F., 1986, "A Stewart Platform-Based Manipulator: General
Theory and Practical Construction,"*The International Journal of Robotics*
Research , Vol. 5, No. 2   ,

[12] Fichter, E.F., McDowell, E.D., 1980, "A Novel Design for a Robot
Arm," *Advances in Computer Technology,* an ASME Publication

[13] McCallion, H., Truong, P.D., 1980, "The Analysis of a Six-Degree-of-
Freedom Work Station for Mechanised Assembly," *Proceedings of the*
Fifth World Congress on Theory of Machines and Mechanisms, an ASME
Publication

[14] Tanner, A.B., 1987, *Study of Robotic Manipulators Subjected to Base Disturbances*, M.S. Thesis, MIT, Cambridge, MA

[15] Vafa, Z., 1987, *The Kinematics, Dynamics and Control of Space Manipulators: The virtual Manipulator concept*, Ph.D. Thesis, MIT, Cambridge, MA

[16] Weng, T.C., Sandor, G.N., Xu, Y., Kohli, D., 1987, "On the Workspace of Closed-Loop Manipulators with Ground-Mounted Rotary-Linear Actuators and Finite Size Platform," *Proceedings of the 1987 ASME Design Tech., Vol. II, Robotics, Mechanisms and Machine Systems,* Boston, MA, Sept. 27-30

[17] Yang, D.C.H., Lee, W.L., 1989, "Feasibility Study of a Platform Type of Robotic Manipulators from a Kinematic Viewpoint," *Transactions of ASME Journal of Mechanisms, Transmission and Automation in Design,* Vol. 106

[18] Griffis M, Duffy, J., 1989, "A Forward Displacement Analysis of a Class of Stewart Platforms" *Journal of Robotic Systems,* Vol. 6,.No. 6, pp. 703-720

[19] Nanua, P., Waldron, K.J., 1990, "Direct Kinematic Solution of a Stewart Platform" *IEEE Transactions on Robotics and Automation,* Vol. 6,.No. 6, pp. 438-444

[20] Sugimoto, K., 1986, "Kinematic and Dynamic Analysis of Parallel Manipulators By Means of Motor Algebra" *ASME Paper,* .No. 86-DET-139

[21] Zhang, C., Song, S 1991, "Forward Kinematics of A Class of Parallel (Stewart) Platform with Closed-Form Solutions", *Proceedings of 1991 IEEE International Conference on Robotics and Automation,*.Sacramento, CA, April, pp. 2676-2682

[22] Cleary, K., Arai, T 1991, "A Prototype Parallel Manipulator: Kinematics, Construction, Software, Workspace Results, and Singularity Analysis", *Proceedings of 1991 IEEE International Conference on Robotics and Automation,*.Sacramento, CA, April, pp. 566-571

[23] Cwiakala, M, 1986, "Workspace of a Closed-Loop Manipulator", *ASME Paper,*.No. 86-DET-95

[24] Gosselin, C., 1990, "Determination of the Workspace of 6-DOF Parallel Manipulators", *Transactions of the ASME Journal of Mechanical Design,*.Vol. 112, Sept. pp. 331-336

[25] Gosselin, C., 1990,, "Singularity Analysis of Closed-Loop Kinematic Chains", *IEEE Transactions on Robotics and Automation,*.Vol. 6, No. 3, June, pp. 377-290

[26] Gosselin, C., 1990,, "Stiffness Mapping for Parallel Manipulators", *IEEE Transactions on Robotics and Automation,.*Vol. 6, No. 3, June, pp. 377-388

[27] Nguyen, C. C, Antrazi, S.S., Campbell, C.E., 1991, "Experimental Study of Motion Control and Trajectory Planning for a Stewart Platform Robot Manipulator", *Proceedings of 1991 IEEE International Conference on Robotics and Automation,.*Sacramento, CA, April, pp. 1873-1878

[28] Stewart, D., 1965-66, "A Platform with Six Degrees of Freedom", *Proceedings of the Institution of Mechanical Engineers,.*Vol. 180, Part 1, No. 15

[29] Ahmad, S., 1988, "Analysis of robot drive train errors, their static effects, and their compensation," IEEE *Int. Conf. Rcbotics and Automation,*

[30] Vuskovic, M., 1989, "Kinematic Sensitivity of Robot Manipulators", *NASA Conference on Space Telerobotics,* Jet Propulsion Laboratory, Pasadena, CA, Jan. 31-Feb. 2

[31] Hollerbach, J. M., and Bennett, D.J., 1988. "Automatic kinematic calibration using a motion tracking system," *Robotics Research: the Fourth International Symposium,* edited by R. Bolles and B. Roth, Cambridge, MA, MIT Press, pp. 191-198

[32] Payannet, D., Alton, M. J., and Liegeois, A., 1985, "Identification and compensation of mechanical errors for industrial robots," *Proc. 15th Int. Symp. on Industrial Robots,* Tokyo, pp. 857-864.

[33] Wu, C.-H., and Lee, C.C., 1984, "On an accuracy problem of robot manipulators," *Proc. 23rd IEEE Conf. decision and Control,* Las Vegas, Dec. 12-14, pp. 1636-1637.

[34] Wu, C.-H., and Lee, C.C., 1985, "Estimation of accuracy of a robot manipulator," *IEEE trans. Automatic Control,* AC-30, pp. 304-306.

[35] Ziegert, J., and Datseris, P., 1988, "Basic considerations for robot calibration," *Proc. IEEE Int. Conf. Robotics and Automation,* Philadelphia, April 24-29, pp. 932-938.

[36] Landsberger, S.E., 1988, *Linear Algebra and Geometry of Velocity and Force Systems with Applications to Mechanisms ,* Sc.D. Thesis, MIT, Cambridge, MA